Rock Mechanics and Rock Engineering
https://doi.org/10.1007/s00603-024-04178-w

ORIGINAL PAPER

Block Volume and Shape: Comparison of Calculation Methods and Investigation of Possible Relationships

Battista Taboni[1] · **Anna Maria Ferrero**[1] · **Gessica Umili**[1]

Received: 26 February 2024 / Accepted: 12 September 2024

Abstract

In dealing with rockfall risk mitigation, a proper assessment of the phenomenon is the key to correctly and precisely managing its possible consequences. In doing so, numerical simulations are an unavoidable step of the assessment process. The proper description of the slope and the falling rock is paramount. Thus, it is highly relevant to accurately assess block size and shape. Block size directly defines the kinetic energy involved in the phenomenon, whilst shape directly influences its trajectory. Tools to properly assess both block size and shape are available, either in analytical form or relying upon Discrete Fracture Network (DFN) models. However, at present, no concrete demonstration of the equivalence of these two methods is provided in the literature. Moreover, block size and shape are always treated separately, while it is likely that a relationship of some sort exists between the two as they derive from the same features of the rock mass (i.e., the 3D geometry of its discontinuities). This paper presents a comprehensive study concerning (1) the comparison between DFN and analytical approaches and (2) the existence and quantification of a shape–size correlation. A modeling campaign consisting of 20 different geometrical structures is performed with both methods, with the aim of obtaining In Situ Block Size Distributions and Shape Distributions. Although the DFN and the analytical approach have different advantages and disadvantages, they have proved to be comparable in terms of results. Both methods identify the existence of a correlation between shape and size of the blocks: the shape distribution changes with reference to block size. This result points out the importance of implementing shape distribution in rockfall numerical simulations. Finally, a suitable case study from the literature has been selected to test the applicability and usefulness of the new findings for the design of rockfall barriers.

Highlights

- In situ block size distribution assessment through different methods.
- Block shape assessment and shape distribution evaluation.
- Investigation of relationships between block size and shape.
- Application to rock fall hazard assessment.

Keywords IBSD · DFN · Block · Volume · Shape · Analytical method

Abbreviations

DFN	Discrete fracture network
AM	Analytical method
IBSD	In situ block size distribution
SD	Shape distribution
SSD	Size–shape distribution
PDF	Probability density function
CDF	Cumulative distribution function
CV	Coefficient of variation
REV	Representative elementary volume
P_{32}	Fracture intensity
Ψ	Expected value (mean) of dip angle of a discontinuity plane
α	Expected value (mean) of dip direction angle of a discontinuity plane

✉ Battista Taboni
battista.taboni@unito.it

[1] Department of Earth Sciences, University of Turin, Via Valperga Caluso 35, 10125 Turin, Italy

Published online: 28 September 2024

σ_Ψ	Variance of dip angle
σ_α	Variance of dip direction angle
S	Spacing, intended for both a deterministic value and a continuous random variable
μ	Expected value (mean) of spacing (coincident with E[S])
σ^2	Variance of spacing (coincident with Var[S])
V	Volume
μ_v	Expected value (mean) of volume
σ_v	Variance of volume
N	Number of data in the spacing or volume sample
E[V]	Expected value (mean) of volume
Var[V]	Variance of volume
K_i, K_j, K_k	Discontinuity sets
S_i, S_j, S_k	Spacing of the three discontinuity sets generating the block
γ_{ij}, γ_{jk}, γ_{ki}	Angles between pairs of discontinuity sets generating the block
$\delta_{k\text{-}ij}$	Angle between K_k and the intersection of K_i and K_j
q	Dimensionless number calculated based on the orientation of the three discontinuity sets generating the block
Lo	Length of the longest edge of the block
In	Length of the intermediate edge of the block
Sh	Length of the shortest edge of the block
$V_{n\%}$	Volume corresponding to $n\%$ cumulative frequency in IBSD (i.e., $V_{99\%}$ corresponds to 99% cumulative frequency of IBSD)
E_k	Total kinetic energy of the block

1 Introduction

In dealing with rockfall risk mitigation, a proper assessment of the phenomenon is key for the correct and precise management of its possible consequences. In doing so, numerical simulations are an unavoidable step of the assessment process: in fact, rockfall hazard assessment involves the statistical analysis of the outputs of a large number of simulations to evaluate, for instance, the variability of the possible runout paths, and consequently to quantify the energies involved (Volkwein et al. 2011). The accuracy of numerical simulations is directly influenced by the accuracy and reliability of the model they are based upon. Therefore, the proper description of the slope and the falling rock are paramount. Focusing exclusively on the rock mass, two of the most influential features, in terms of influence on the propagation of a rockfall event, are block size and shape (Pfeiffer and Bowen 1989).

Block size directly defines the kinetic energy involved in the propagation phase of the phenomenon. It is generally assumed to be one of the most relevant parameters to be assessed and quantified in rockfall hazard analysis. In fact, traditional design methods for protection works are commonly referred to as energy-based (Wyllie 2015). Issues arise from the fact that block size suffers from natural variability as a consequence of the natural variability of the joint spacing and orientation within a given rock mass. Therefore, a single deterministic block size value cannot satisfy the high accuracy and reliability requirements of a proper hazard assessment. To solve this issue, which is not exclusively related to rockfall modeling, but rather to the general description of the geometric features of a rock mass, the concept of In-situ Block Size Distribution (IBSD) was introduced (Wang et al. 1991, 1993; Lu and Latham 1999; Stavropoulou 2014; Umili et al. 2023). This approach allowed to step away from single deterministic values, moving towards a fully probabilistic description of block size, where the variable is presented as a cumulative frequency distribution. Such a distribution can be obtained by means of analytical equations, such as the original definition of IBSD intended: a good overview of the available empirical relations to quantify block volume is presented by Koulibaly et al. (2023). The IBSD can also be assessed by employing a discrete fracture network (DFN) to construct a numerical model of a jointed rock mass: DFNs, as introduced by Baecher (1983), Andersson et al. (1984), and Dershowitz and Einstein (1988), are an intuitive and very powerful tool to assess the geometrical features of a rock mass, directly simulating the discontinuities within a rock volume. An IBSD can be either employed to quantitatively justify the choice of a reference block size value or directly as input for numerical simulations; this means that the IBSD approach can still be employed in the conventional and traditional design approaches while also allowing for more sophisticated techniques to be used (Taboni et al. 2023).

Block shape is a direct consequence of the geometric characteristics of the rock mass, similarly to block size (Mauldon 1994). Shape also plays a significant role, as it directly influences the geometric side of the propagation phase of a rockfall event (i.e., the trajectory of the falling block) and its randomness (Kobayashi et al. 1990). For this reason, in recent years, the scientific literature has produced several works assessing the significance of block shape (Torsello et al. 2021; Caviezel et al. 2021; Umili et al 2023) and the role of proper shape integration within numerical simulations (Bourrier and Acary 2022). Moreover, nowadays, rockfall simulation software capable of integrating block shapes is common, although mainly limited to 3D simulations and with different levels of accuracy and complexity (Pfeifer and Bowen 1989; Dorren 2016; Toe et al. 2018; Leine et al. 2014, 2021; Noël et al. 2016, 2021). Outside of the context of run-out numerical simulations, it should be noted how shape also influences the interaction between the

falling block and existing passive protection works, such as flexible barriers, along its path (Yu et al. 2021). Given that the natural variability of rock mass geometric properties influences block size as well as block shape, a tool to describe block shape variability quantitatively is required. Kalenchuk et al. (2006, 2008), while analyzing block shapes derived from both DFN derived from real case studies and purely synthetic DFN models, found that the actual shapes of the observed blocks can be plotted on a triangular shape classification diagram of their design. An application of this approach is provided by Buyer et al. (2020) and Kong et al. (2021). The same results were also found by Feng et al. (2011). Following a similar approach, Umili et al. (2023) expanded upon this and introduced the Shape Distribution (SD) in the context of rockfall problems; such distribution describes the relative abundance of each shape type with reference to Palmstrom's classification of block shapes (Palmstrom 2001): the intent was to provide an easy-to-reproduce analytical methodology, based upon a simplification of the actual geometry of the problem. In fact, the blocks are assumed to be orthogonal prisms, i.e., all sides are normal or very close to normal with respect to each other. Under this assumption, the distance between the opposite faces of the prism, namely the spacing between planes belonging to the same discontinuity set, corresponds to the edge length. Therefore, the spacing distributions of the three joint sets also describe the prism edges. The shape classification selected to visualize the distribution is actually irrelevant, as the methodology works in any case. Thus, it can be seen that it is possible to derive a relative frequency distribution both from DFN models and analytical methods. It should be kept in mind that DFN models require the assessment of the Representative Elementary Volume (REV) to model any real case properly (Zhou et al. 2022; Huang et al. 2024). Such a distribution can be used to define a reference shape for numerical simulations (i.e., the most frequent one) if the distribution features one clearly dominant shape type. Alternatively, one can perform as many sets of numerical simulations as the considered shape classes and weight the results based on their relative frequency. Such an approach is presented by Taboni et al. (2023), providing also a practical application.

Thus, it is clear that tools to assess both block size and shape properly are available, either in analytical form or relying upon DFN models. Theoretically, both methods should yield similar or very similar results, given the same input data. In practice, to the best of the authors' knowledge, no concrete demonstration of this fact is provided in the literature. It also appears quite evident that relying on DFNs is significantly more common than employing analytical approaches when dealing with rock mass characterization and instability, independently of the scale of the phenomena (Bhusan et al. 2020; Wang and Cai 2020; Zhang et al. 2021; Singh et al. 2022; Fan et al. 2023;). Moreover, the two block features, namely size and shape, are always treated separately for the sake of simplicity. In reality, though, it is likely that a relationship of some sort exists between the two features, as they both depend on the same geometrical parameters (i.e., spacing and orientation of joints). As a matter of fact, both Kalenchuk et al. (2006, 2008) and, consequently, Umili et al. (2023) pointed out that when plotting the distribution of shapes with regard to the corresponding size of each plotted block, a trend is visible: the larger the volume, the higher the likelihood of an equidimensional shape.

In this paper, the authors present a comprehensive study concerning (1) the comparison between DFN and analytical approaches, highlighting the similarity of the results, methodological differences, and advantages or limitations; (2) the existence and quantification of a shape–size correlation. A modeling campaign consisting of 20 different geometrical structures is performed with both methods, with the aim of obtaining IBSDs and SDs. Although the DFN and the analytical approach have different advantages and disadvantages, they have proved to be comparable in terms of results. Finally, a suitable case study from the literature has been selected to test the applicability and usefulness of the new findings for the design of rockfall barriers.

2 Materials and Methods

2.1 Block Volume Assessment

The DFN approach provides the three-dimensional description of a rock mass discrete features. In fact, the geometrical structure of a rock mass can be modeled by employing DFN software: a defined volume is assumed as the box containing the rock mass. The input discontinuity sets, along with their geometrical features (i.e., orientation and spacing), control the number, size, and shape of the blocks constituting the model. Theoretically, an equivalent result can be obtained through an analytical approach based on the same input variables: in this case, however, the model is not explicitly or graphically created and, therefore, is not visible in a defined space; this method provides only a list of geometrical features, not associated with specific coordinates in the space. In both cases, the natural variability of the geometrical features in the rock mass can be modeled by associating frequency distributions to the orientation and spacing input data of the main discontinuity sets.

Sections 2.1.1 and 2.1.2 contain a detailed explanation of both methods.

2.1.1 DFN-Based Method for Volume Assessment

A DFN creates a 3D box representing the intact rock matrix and, through specific commands, cuts it into blocks by interrupting its continuity along planes. A discontinuity set in the rock mass is modeled as a group of planes, by inputting the mean orientation, usually expressed by dip (Ψ) and dip direction (α) and their variability (σ_ψ, σ_α), the mean spacing (μ), and its variability (σ). In the research work presented here, the authors used 3DEC (ITASCA 2007) as a DFN: three perpendicular discontinuity sets were input to create regular blocks of six faces each. The choice of not assigning a variability to the orientation, combined with the adoption of fully persistent planes, was made to focus the attention on the effect of the variability of the spacing only. In this regard, spacing of the three sets was set to vary both in terms of μ and σ. 3DEC's manual states that the input σ is used to assign a random deviation for each cut, generated by a call to a random number generator. This fact corresponds to the adoption of a Normal PDF.

The aim of utilizing a DFN in this work is to create the IBSD under specific input conditions. However, since the modeled volume is finite, the ratio between block volumes and model volume influences the representativeness of the results. In other words, it is of fundamental importance to find the REV. With reference to jointed rock masses, the REV can be defined as the volume of investigated rock containing enough discontinuities and inhomogeneities so that the global average value is consistent for repeated measurements (Esmaieli et al. 2010). The value of REV for a given case can be easily assessed with a diagram such as the one proposed by Hudson and Harrison (1997), where a variable is plotted against the reference volume in order to identify the REV size.

Therefore, the first series of experiments were designed to model five rock masses, each affected by the presence of three perpendicular discontinuity sets, characterized by five different triplets of average spacing values (μ_1, μ_2, μ_3) and null standard deviation ($\sigma_1=\sigma_2=\sigma_3=0$). Each triplet is associated with a constant expected volume E[V] and a different expected block shape. Based on the chosen E[V], a series of cubic models with increasing edge length are generated to find the REV. For each of these models, the block list is extracted to build the IBSD and calculate the average block size μ_v and the corresponding block size standard deviation σ_v. The theoretical IBSD for each of these models is represented by a vertical line extending from 0 to 100%, whose abscissa is equal to E[V]. The choice of REV, namely the choice of the model edge length, is based on the comparison of the obtained IBSDs with the theoretical one; moreover, other criteria consist of the analysis of the trends of μ_v and σ_v, to assess the minimum model edge length for which the influence of model size becomes negligible on the results.

Once the REV is assessed, a further series of analyses can be carried out to assess the influence of spacing variability on the IBSD and SD. For this purpose, the same spacing triplets as in the first series of models are considered, and three increasing standard deviations are assumed. In this way, a total of 20 volume distributions will be obtained from the generated models.

2.1.2 Analytical Method for Volume Assessment

The analytical method (AM) here tested is based on the definition of IBSD introduced by Umili et al. (2023). It adopts the equation for calculating block volume proposed by Umili et al. (2024), which has been proven to be geometrically correct

$$V = \frac{S_1 S_2 S_3}{q}, \tag{1}$$

where S_1, S_2, and S_3 are the average spacing values of the three discontinuity sets generating the block. The coefficient q is a dimensionless number that depends only on the relative orientation of the three joint sets defining the block, namely the angles between normal vectors; it can be calculated as

$$q = sin\gamma_{12}\cos\delta_{3-12} = sin\gamma_{23}\cos\delta_{1-23} = sin\gamma_{31}\cos\delta_{2-31}, \tag{2}$$

where γ_{12} is the angle between K1 and K2, and $\delta_{3\text{-}12}$ is the angle between K3 and the intersection of K1 and K2. If the block is a regular prism whose angles among sets are all equal to 90°, q is equal to 1.

Briefly, the analytical definition of the IBSD is based on the assumption that the spacing of a discontinuity set is a continuous random variable, which means that its CDF, denoted as $F(s)=P(S\leq s)$, defines the probability that a given spacing value S is less than s (Stavropoulou 2014). By adopting Eq. 1 and assuming that the spacing distributions of the three discontinuity sets are independent, the CDF of the block volume can be written as

$$F_V(v) = \frac{F_{S_1}(s_1)F_{S_2}(s_2)F_{S_3}(s_3)}{q}, \tag{3}$$

which represents the analytical definition of the IBSD.

Under the assumption of constant q ($E[q]=q$, $Var[q]=0$), Umili et al. (2023) demonstrate that it is possible to explicitly calculate the expected value and variance of the volume as follows:

$$E[V] = \frac{\mu_1\mu_2\mu_3}{q} \tag{4}$$

$$\mathrm{Var}[V] = \mu_1^2\mu_2^2\sigma_3^2 + \mu_1^2\mu_3^2\sigma_2^2 + \mu_2^2\mu_3^2\sigma_1^2 + \mu_3^2\sigma_1^2\sigma_2^2 + \mu_1^2\sigma_2^2\sigma_3^2 + \mu_2^2\sigma_1^2\sigma_3^2 + \sigma_1^2\sigma_2^2\sigma_3^2. \quad (5)$$

Equation (3) provides an average value of the volume, while Eq. (4) provides the variance of the volume, considering the combined effects of spacing variability, both in terms of mean and variance.

To compare the results with those obtained with the DFN models, the same PDF distribution type (i.e., normal) and the same parameters (μ and σ) are adopted for randomly generating sets of spacing values, with which to calculate volume samples and build the corresponding IBSDs.

It should be stressed, though, that the analytical approach is applicable as presented here only if no more than three joint sets are present; if this is not the case, a combinatory approach is suggested. In this regard, a DFN approach is more flexible.

2.2 Block Shape Assessment

Following a similar approach, it is possible to define a Shape Distribution (SD), with reference to a given block size distribution. This tool allows for a proper assessment of block shape within a given case study. The SD can be computed from the block features identified in a DFN model, as was done by Kalenchuk et al. (2006, 2008); alternatively, it is possible to compute the SD by assuming that the joint sets are reciprocally orthogonal and employing their spacing frequency distributions as descriptors for edge length, as was suggested by Umili et al. (2023) and Taboni et al. (2023). To compare the results of the DFN and the AM, the same classification system and diagram were used: for its simplicity and ease of calculation, we selected Palmstrom's classification (Palmstrom 2001). Such a classification defines four shape types, depending on the ratios between the length of the longest (Lo), intermediate (In), and shortest (Sh) edge of a block. The corresponding logarithmic diagram is, thus, divided into four sectors according to the following definitions:

- Equidimensional or compact prisms, with In/Sh < 2 and Lo/Sh < 2;
- Long prisms (rods), with In/Sh < 2 and Lo/Sh > 2;
- Long flat prisms (blades), with 2 < In/Sh < 1 + (Lo/Sh–1)^0.5;
- Flat prisms (slabs), In/Sh > 1 + (Lo/Sh–1)^0.5.

Given that any classification system relies upon arbitrary boundaries to define its classes, it is easy to understand that an SD can present itself differently for different shape classifications. The existence of the SD, though, is independent of its representation on a diagram.

2.2.1 DFN-Based Method for Shape Assessment

For each of the DFN models created, the list of vertices of each block, consisting of an identification number and its coordinates (*X*, *Y*, *Z*), is automatically extracted. The list is used to calculate the length of the six edges of each block. Due to the choice of three perpendicular sets, the edges with unique values are three for each block. They are then used to calculate the ratios In/Sh and Lo/Sh and plot the relative points on the shape diagram.

2.2.2 Analytical Method for Shape Assessment

Based on the same samples of spacing values used to build the IBSD with the AM, it is possible to calculate the ratios In/Sh and Lo/Sh for each block and plot the relative points on the shape diagram.

3 Calculation of the Required Data

3.1 Choice of Input Data

The choice of input data for generating the blocks is bound, on the one hand, by the need to use only three discontinuity sets to fulfill the requirements of the AM. On the other hand, it is constrained by the need to have perpendicular discontinuity sets to create regular blocks of six faces each and use the shape definition by Palmstrom (2001). Moreover, as described in Sect. 2.1.1, the need to assess the influence of spacing variability on the IBSD and SD must be coupled with the identification of the REV for the DFN models.

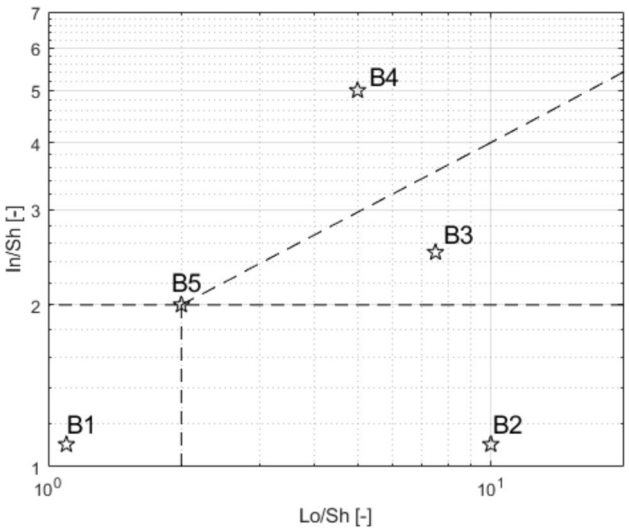

Fig. 1 Shape diagram with the five chosen combinations B1, B2, B3, B4, and B5

Table 1 Orientation and spacing data assumed for each of the five combinations

Combination	K1			K2			K3		
	Orientation [°]	Spacing [m]		Orientation [°]	Spacing [m]		Orientation [°]	Spacing [m]	
	Ψ_1/α_1	μ_1	σ_1	Ψ_2/α_2	μ_2	σ_2	Ψ_3/α_3	μ_3	σ_3
B1	90/000	1.71	0	90/090	1.71	0	00/000	1.71	0
	90/000	1.71	0.1	90/090	1.71	0.1	00/000	1.71	0.1
	90/000	1.71	0.2	90/090	1.71	0.2	00/000	1.71	0.2
	90/000	1.71	0.5	90/090	1.71	0.5	00/000	1.71	0.5
B2	90/000	0.77	0	90/090	0.85	0	00/000	7.69	0
	90/000	0.77	0.1	90/090	0.85	0.1	00/000	7.69	0.1
	90/000	0.77	0.2	90/090	0.85	0.2	00/000	7.69	0.2
	90/000	0.77	0.5	90/090	0.85	0.5	00/000	7.69	0.5
B3	90/000	0.64	0	90/090	1.61	0	00/000	4.83	0
	90/000	0.64	0.1	90/090	1.61	0.1	00/000	4.83	0.1
	90/000	0.64	0.2	90/090	1.61	0.2	00/000	4.83	0.2
	90/000	0.64	0.5	90/090	1.61	0.5	00/000	4.83	0.5
B4	90/000	0.58	0	90/090	2.92	0	00/000	2.92	0
	90/000	0.58	0.1	90/090	2.92	0.1	00/000	2.92	0.1
	90/000	0.58	0.2	90/090	2.92	0.2	00/000	2.92	0.2
	90/000	0.58	0.5	90/090	2.92	0.5	00/000	2.92	0.5
B5	90/000	1.08	0	90/090	2.15	0	00/000	2.15	0
	90/000	1.08	0.1	90/090	2.15	0.1	00/000	2.15	0.1
	90/000	1.08	0.2	90/090	2.15	0.2	00/000	2.15	0.2
	90/000	1.08	0.5	90/090	2.15	0.5	00/000	2.15	0.5

For these reasons, five spacing triplets (μ_1, μ_2, μ_3) representative of five different points on the shape diagram are chosen (Fig. 1): they will be referred to as combinations B1, B2, B3, B4, and B5 (Table 1). All the combinations are characterized by the same orientation of the three mutually perpendicular sets (K1, K2, K3) and by an identical expected block volume E[V] (Eq. 4) equal to 5 m^3. According to the shape diagram, B1 is an equidimensional block, B2 a rod-like one, B3 a blade-like block, and B4 a slab-like one; lastly, B5 describes the common point between all shapes, identified by the intersection of the lines dividing the diagram into the different shape sectors.

For each combination, a null and three increasing σ values (0.1, 0.2, 0.5 m) are assumed. A total of 20 sets of data were created and inputted both in DFN and AM, to perform a broad comparison of the results.

3.2 REV Identification

The input data of the five combinations (Table 1) are designed to produce DFN models with the same E[V], once the REV is adopted. In light of this fact, combination B1 is used to assess the REV. B1 represents a cube whose edge length is 1.71 m. The model edge length is varied from 10 m to 45 m (Table 2): this means that the cubic models will theoretically contain 200 to 18225 blocks. By comparing the IBSDs obtained for the different edge lengths, it is possible to note that the curves tend to coincide with the theoretical one as the dimension

Table 2 Cube dimension and rock block volumes for Combination B1 (σ = 0)

Edge length [m]	Number of blocks		Block volume			
	Theoretical	Actual	Maximum [m^3]	Minimum [m^3]	Average value [m^3]	Variance [m^6]
10	200	343	5	0.06	2.92	3.22
20	1600	2197	5	0.02	3.64	3.25
30	5400	6859	5	0.01	3.94	3.13
35	8575	9261	5	0.78	4.63	0.67
40	12,800	13,824	5	0.30	4.63	1.01
45	18,225	19,683	5	0.49	4.63	0.74

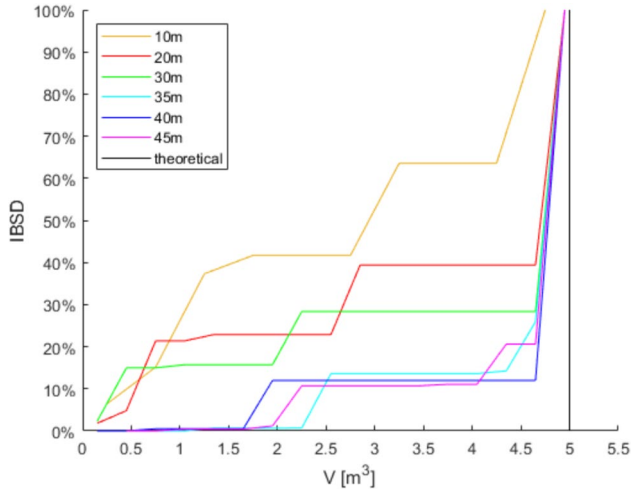

Fig. 2 Comparison of IBSDs obtained for different values of model edge length

increases (Fig. 2). The actual number of blocks in the models converges to the theoretical one with increasing edge length: from 35 m, the difference remains stable at +8% with respect to the theoretical number. Moreover, by comparing the mean μ_v and standard deviation σ_v of the block samples generated by 3DEC models with increasing edge length (Figure 3), one can observe a marked variation of both trends in correspondence with the model edge length equal to 35 m.

Similar considerations can be made based on fracture intensity P_{32}, which is defined as the ratio of the total area of discontinuities and the volume of the rock mass considered (Zhang and Einstein 2000)

$$P_{32} = \frac{1}{V}\sum_{k=1}^{m^{(V)}} S^{(k)}, \tag{7}$$

where V is the volume of the rock mass considered; $S^{(k)}$ is the entire area of the kth discontinuity; $m^{(V)}$ is the number of discontinuities (i.e., the number of discontinuity centroids) in volume V.

Values of P_{32} of the DFN models, created with edge lengths from 10 to 45 m for each of the five combinations B1–B5, are calculated: Fig. 4 depicts them. Considering this estimator, too, all the trends agree and show that from 35 m edge length, values are reasonably stable as they manifest an asymptotic trend.

In light of these observations, a dimension of the virtual rock mass of 35 m was chosen for the following analyses as the REV.

3.3 DFN and AM Models Generation

The DFN was used to produce the 20 designed models based on the data in Table 1. For each model, the lists of the vertices and block volumes were extracted and processed to build the IBSD and SD. Based on the number of blocks (N) obtained for a DFN model, the corresponding AM model is generated, so that it consists of N spacing data for each discontinuity set and, consequently, N blocks.

Matlab function *normrnd* is used to generate samples of random numbers from the Normal distribution, by inputting mean parameter (μ), standard deviation parameter (σ), and the number of values to be generated (N).

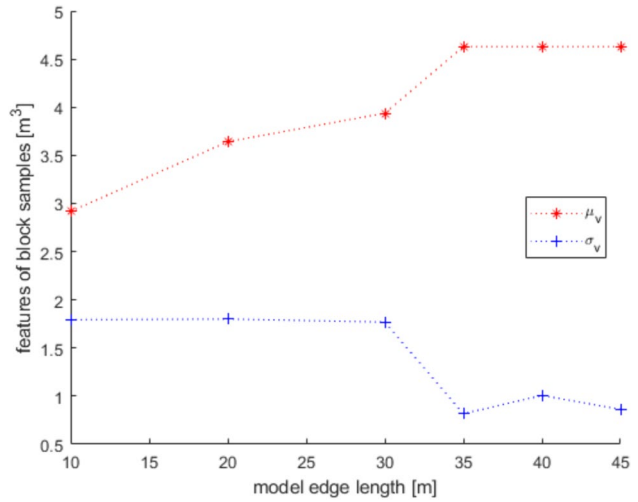

Fig. 3 Mean μ_v and standard deviation σ_v of the block samples generated by 3DEC models with increasing edge length

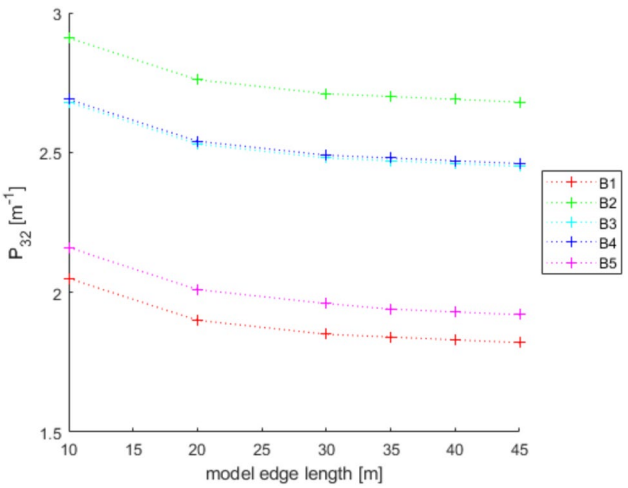

Fig. 4 Values of P_{32} calculated for the models generated by 3DEC with increasing edge length

4 Results and Discussion

Since the models created through DFN and AM have the same input data, the first step for a comprehensive comparison of the results is the analysis of their raw output values. In other words, due to the fact that, in this study, block volume is the product of three spacing values, the first check must be on the ability of the two methods to produce the expected spacing values. Considering that the input data (Table 1) describe the theoretical and, therefore, true PDF, it is possible to describe the obtained sample by means of its average value μ* and standard deviation σ*. Defining Δ the difference between the coefficients of variation CV* and CV

$$\Delta = CV^* - CV = \frac{\sigma^*}{\mu^*} - \frac{\sigma}{\mu}, \tag{8}$$

one can assess a normalized difference between the true PDF and the sample PDF: Δ equal to 0 represents complete equality. Figure 5 shows the Δ values obtained considering both methods: in general, values obtained with AM are closer to 0, particularly for small σ and μ greater than 1.5 m. This means that the process of values generation is rigorous, repeatable, and reliable. It is also evident that the spacing samples generated by the DFN suffer from an effect of truncation due to the actual process of subdivision of the model by means of discontinuity planes. The generated spacing samples show a more chaotic behavior of Δ, due mainly to a greater difference between the obtained σ* and the true σ.

The analysis of spacing samples is essential for the investigation and assessment of volume samples. In fact, the effect of μ* and σ* deviation from μ and σ is reflected in the difference among the volume PDFs. The theoretical E[V] and Var[V] calculated with Eqs. 4 and 5 can be compared to those calculated based on block samples obtained using the DFN and AM approaches (Table 3). As expected and based on data reported in Fig. 5, the PDF obtained with the AM is closer to the theoretical one than the DFN one. This fact is true regardless of the σ value.

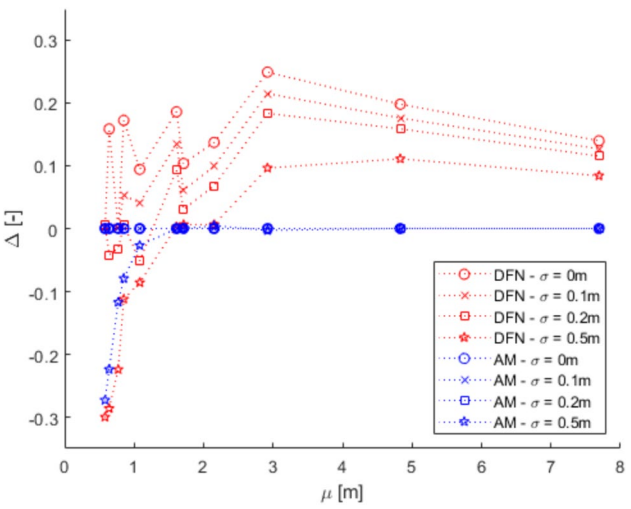

Fig. 5 Comparison between Δ calculated with DFN and AM for different values of σ

4.1 Block Size

The results produced by the methodologies presented in Sects. 2.2.1 and 2.2.2 for the DFN approach and the AM one, respectively, are visible in Fig. 6: DFN derived IBSD on the left, AM calculated IBSD on the right. The results are divided according to the expected shape class of the blocks, as named in Fig. 1. In each diagram, four IBSDs are portrayed to show the effect of increasing σ in the three parent spacing distributions.

First of all, it can easily be appreciated that the AM IBSD tends to cover a wider range of volumes. This is especially visible at high σ values (i.e., 0.5 m), and for the B2 and B3 blocks (rod- and blade-like shapes, respectively). In fact, the maximum volume computed by 3DEC in the case of B3 is roughly equal to 18 m^3, while for the same case, the analytical solution reaches a maximum volume of 35 m^3. This can be interpreted as a consequence of the fact that 3DEC, or any DFN software for that matter, works on a model of pre-defined volume, which has to be equal to or greater than the REV to describe the rock mass geometric properties adequately. This induces an unavoidable limitation on the size of blocks the DFN can identify, as they have to be smaller than the aforementioned pre-defined volume. Such a limitation is absent in the case of the analytic approach, which, on the contrary, can benefit from the definition of a reasonable upper volume limit: Umili et al. (2023) proposed to use $V_{99\%}$, i.e., the volume corresponding to 99% probability of not being exceeded.

A second feature of note, exclusively found on the DFN IBSDs, is the odd segmented curve describing low σ (i.e., 0 or 0.1 m) block size distributions. This odd curve shape is related, once again, to the pre-defined volume of the model within which the DFN computes the rock mass properties; particularly, it is a consequence of how exactly the model can be divided by the discontinuities with the assigned spacing. In other words, when the discontinuities cut the model volume to define the rock mass fracture network, the blocks along the boundaries of the model are defined in geometry (i.e., size and shape) not only by the discontinuities (i.e., their spacing and orientation) but also by the model boundaries themselves. This leads to a surplus of artificially smaller blocks, which alter the trend described by the larger blocks and, thus, the IBSD. The smaller the blocks, the more noticeable this trend: this is why the larger

Table 3 Expected value and variance of the theoretical volume PDF (calculated through Eqs. 4 and 5), expected value, and variance of the block samples obtained through DFN-based and AM, for the combinations B1–B5 and the four considered σ values

		Theoretical PDF		DFN PDF		AM PDF	
		Equation 4	Equation 5				
Id	σ	E[V]	Var[V]	E[V]	Var[V]	E[V]	Var[V]
	m	m^3	m^6	m^3	m^6	m^3	m^6
B1	0	5.00	0.00	4.63	0.67	5.00	0.00
	0.1	5.00	0.26	4.63	0.89	5.00	0.26
	0.2	5.00	1.04	4.61	1.26	5.00	1.03
	0.5	5.00	6.98	4.29	5.79	4.99	6.89
B2	0	5.03	0.00	4.38	1.04	5.03	0.00
	0.1	5.03	0.79	4.40	1.35	5.04	0.76
	0.2	5.03	3.23	4.42	2.62	5.02	3.24
	0.5	5.03	23.35	4.59	9.85	5.85	20.93
B3	0	4.98	0.00	4.16	1.65	4.98	0.00
	0.1	4.98	0.71	4.24	1.69	4.97	0.72
	0.2	4.98	2.89	4.24	3.12	5.02	2.85
	0.5	4.98	19.43	4.50	8.76	5.76	15.27
B4	0	4.95	0.00	4.16	2.26	4.95	0.00
	0.1	4.95	0.79	4.16	2.61	4.94	0.80
	0.2	4.95	3.17	4.16	4.36	4.97	3.22
	0.5	4.95	20.71	4.38	10.04	5.98	14.74
B5	0	4.99	0.00	4.50	0.91	4.99	0.00
	0.1	4.99	0.32	4.50	1.13	5.00	0.33
	0.2	4.99	1.30	4.50	1.50	5.00	1.30
	0.5	4.99	8.70	4.45	5.60	5.10	8.51

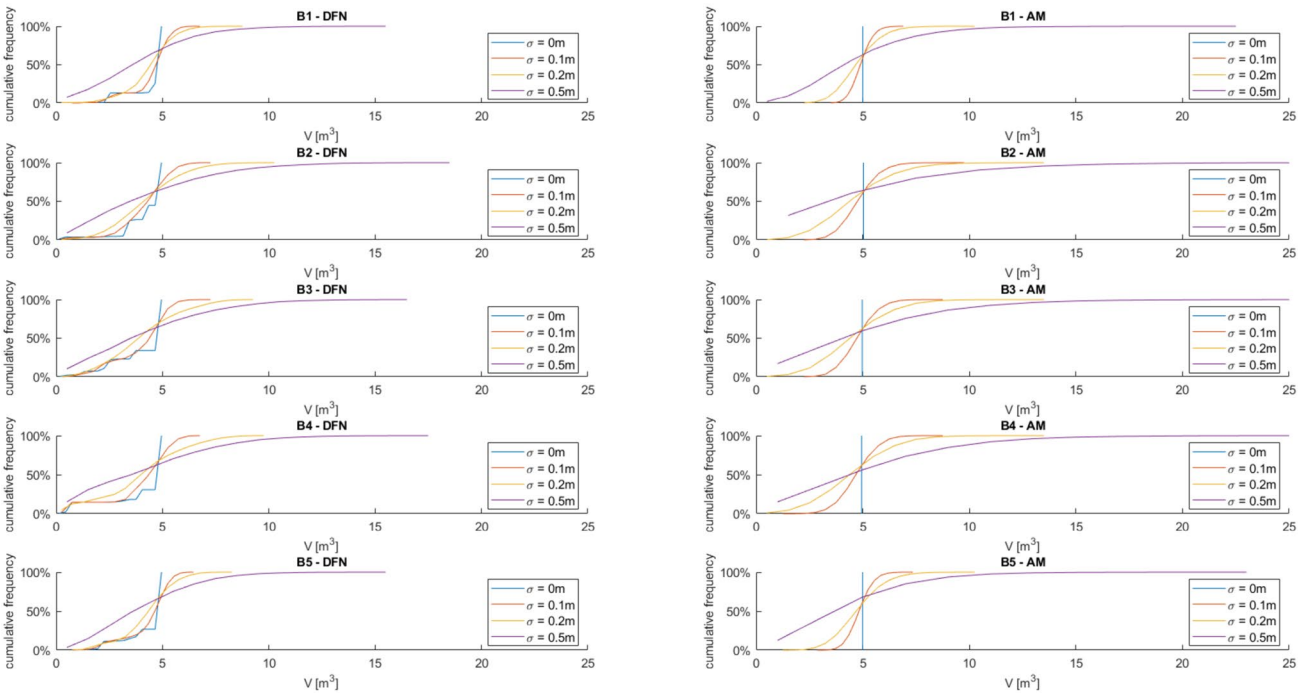

Fig. 6 IBSDs derived from both approaches for different values of σ in the three parent spacing distributions

volume portion of the distributions is not affected. It should also be clear that the boundaries of the modeled volume can only reduce block size. The effect of this feature is clearly distinguishable only for low σ values: less than 0.1 m in our examples. The value of σ of the parent spacing distributions describes how dispersed, and therefore variable, the dataset is. In fact, as the dispersion of spacing increases, the likelihood of the appearance of smaller blocks increases as well, meaning that the presence of boundary-caused small blocks is, at least partially, masked in the appearance of the IBSD curve. The odd appearance of the IBSD curve can be removed by filtering out values below the expected one: this is conceptually fine, though, only for very small σ, as the block size value range is similarly small, and the IBSD tends towards a straight line. In all other instances, filtering out small blocks will also remove actual small blocks computed by the model. As the analytic approach does not rely on an REV or pre-defined model volume, such issues are absent from the AM-derived IBSDs.

Apart from these two features, the IBSDs presented in Fig. 6 appear remarkably similar: although a complete and exact identity between the results of the two approaches is unlikely, given that they are based on different principles and assumptions, the similarity is still significant. To express this fact, Table 4 describes the values at 50%, 75%, and 95% cumulative frequency provided for each model by the two approaches. The difference between volumes at 50% of cumulative frequency calculated with AM and DFN is expressed as $\Delta V_{50\%}$. Similarly, $\Delta V_{75\%}$ and $\Delta V_{95\%}$ consider results obtained for 75% and 95% cumulative frequency, respectively.

As can be seen, these selected frequencies along the IBSDs yield very close results between the two methods. The difference can be quantified considering, for all the five shapes (B1–B5), the same σ value: by entering the relative IBSDs with the considered cumulative frequency, the corresponding volumes can be inferred and the average value calculated. The difference so calculated varies from 0.3 to 0.4 m^3 for $V_{50\%}$, regardless of σ. The difference ranges between 0.2 and 0.8 m^3 for $V_{75\%}$, highlighting a more significant effect of the increase of σ on the increase of the difference. The maximum difference occurs for $V_{95\%}$, as can be noticed by comparing the right tails of the IBSDs: it ranges from 0.1 to 2.2 m^3 by increasing σ, confirming that the AM tends to produce wider IBSDs. This fact supports the choice of adopting $V_{99\%}$ (Umili et al. 2023) as the maximum value for truncating the IBSD.

Table 4 Comparison of the block size values at 50%, 75%, and 95% of cumulative frequency ($V_{50\%}$, $V_{75\%}$, and $V_{95\%}$, respectively) for all the models and both methodologies. ΔV represents the difference between the results of the AM and DFN methods

		DFN			AM			$\Delta V = V_{AM} - V_{DFN}$		
	σ	$V_{50\%}$	$V_{75\%}$	$V_{95\%}$	$V_{50\%}$	$V_{75\%}$	$V_{95\%}$	$\Delta V_{50\%}$	$\Delta V_{75\%}$	$\Delta V_{95\%}$
	[m]	[m^3]	[m^3]	[m^3]	[m^3]	[m^3]	[m^3]	[m^3]	[m^3]	[m^3]
B1	0	4.7	4.8	4.9	5.0	5.0	5.0	0.3	0.2	0.1
	0.1	4.7	5.1	5.6	4.9	5.2	5.8	0.2	0.2	0.1
	0.2	4.4	5.1	6.1	4.7	5.4	6.6	0.2	0.3	0.4
	0.5	3.6	5.3	8.2	4.1	6.0	9.4	0.5	0.7	1.2
B2	0	4.7	4.8	4.9	5.0	5.0	5.0	0.4	0.2	0.1
	0.1	4.3	5.0	5.7	4.7	5.4	6.4	0.5	0.4	0.6
	0.2	4.1	5.2	7.0	4.4	5.7	7.8	0.3	0.4	0.8
	0.5	3.5	6.0	10.2	3.4	6.7	13.1	-0.1	0.7	2.9
B3	0	4.7	4.8	4.9	5.0	5.0	5.0	0.3	0.1	0.0
	0.1	4.4	4.9	5.6	4.7	5.3	6.2	0.3	0.4	0.6
	0.2	3.9	5.2	7.2	4.4	5.6	7.5	0.5	0.5	0.3
	0.5	3.5	5.9	9.6	4.1	6.9	12.3	0.6	1.0	2.7
B4	0	4.7	4.8	4.9	4.9	4.9	4.9	0.2	0.1	0.0
	0.1	4.3	5.0	5.7	4.7	5.3	6.2	0.3	0.3	0.5
	0.2	4.0	5.3	7.4	4.4	5.6	7.5	0.4	0.3	0.1
	0.5	3.5	6.0	9.7	4.4	7.3	12.4	0.9	1.2	2.7
B5	0	4.7	4.8	4.9	5.0	5.0	5.0	0.2	0.1	0.1
	0.1	4.6	5.1	5.6	4.8	5.2	5.8	0.2	0.2	0.3
	0.2	4.3	5.1	6.2	4.7	5.5	6.8	0.4	0.4	0.6
	0.5	3.6	5.5	8.3	3.7	5.8	9.6	0.1	0.3	1.3

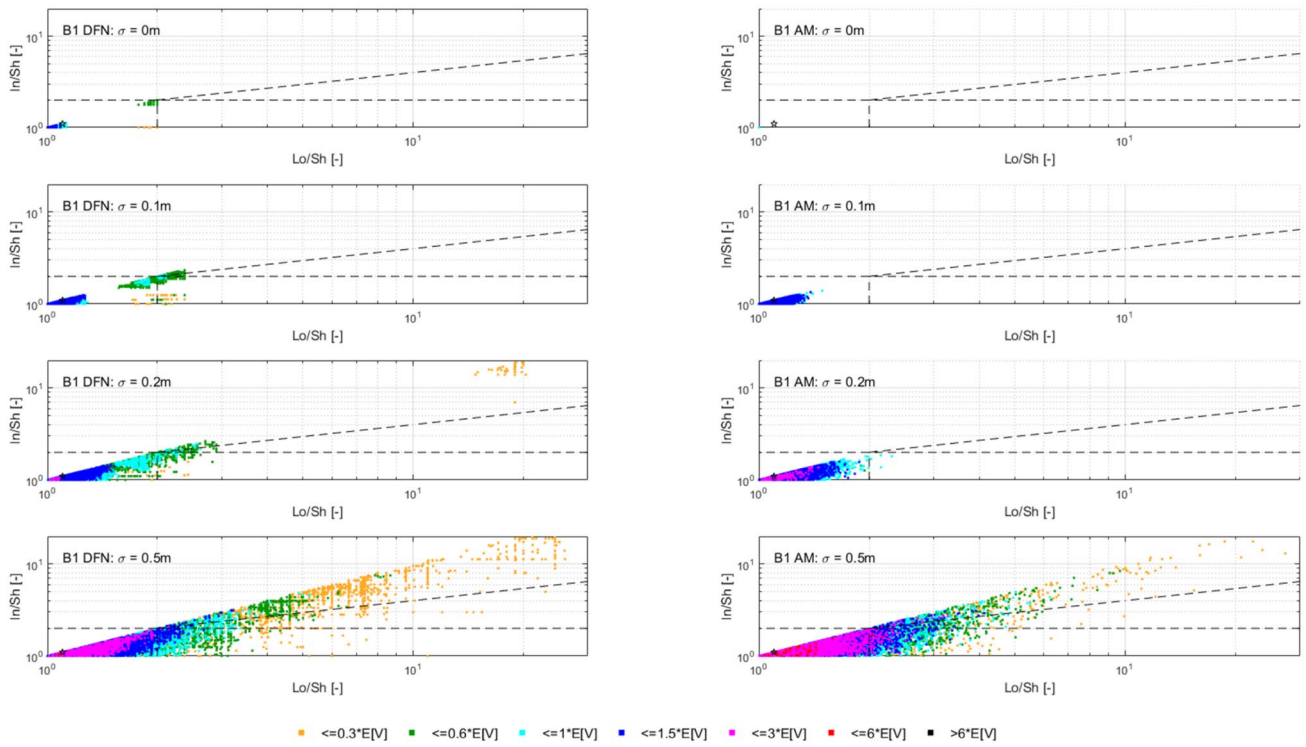

Fig. 7 Computed SDs in the case of reference block B1

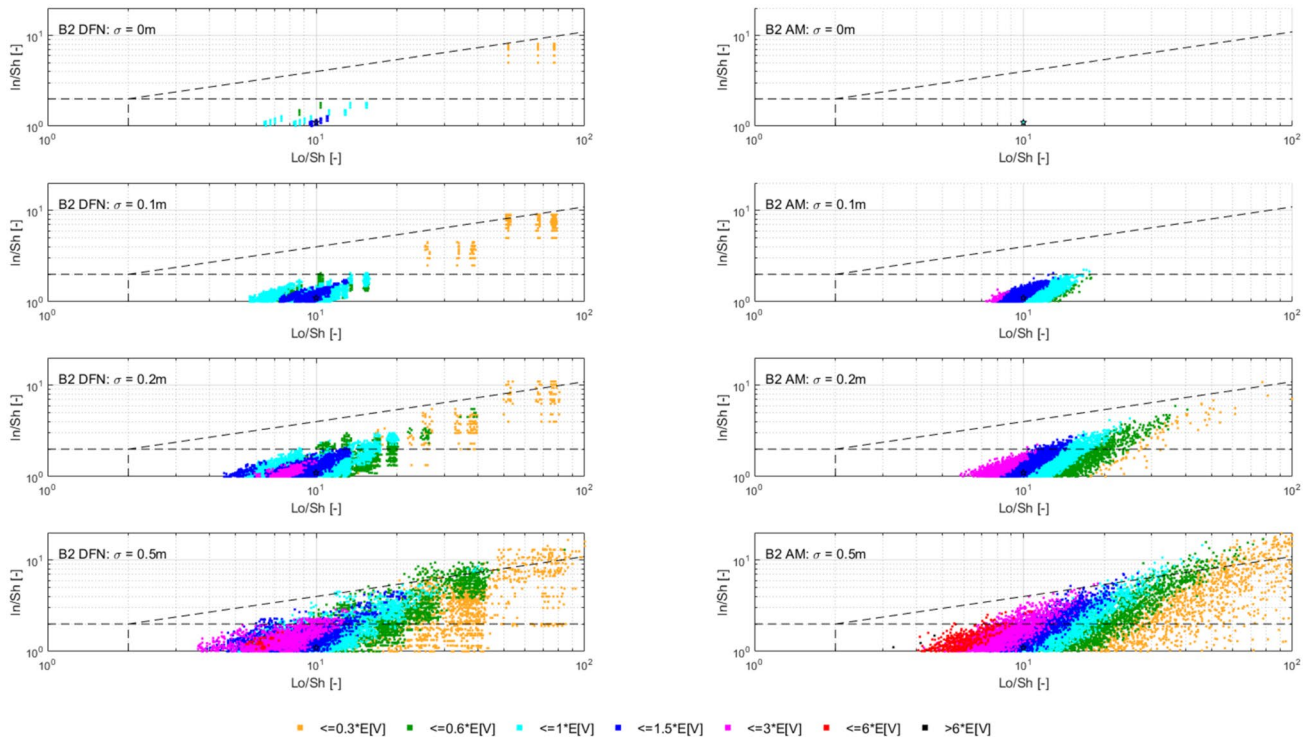

Fig. 8 Computed SDs in the case of reference block B2

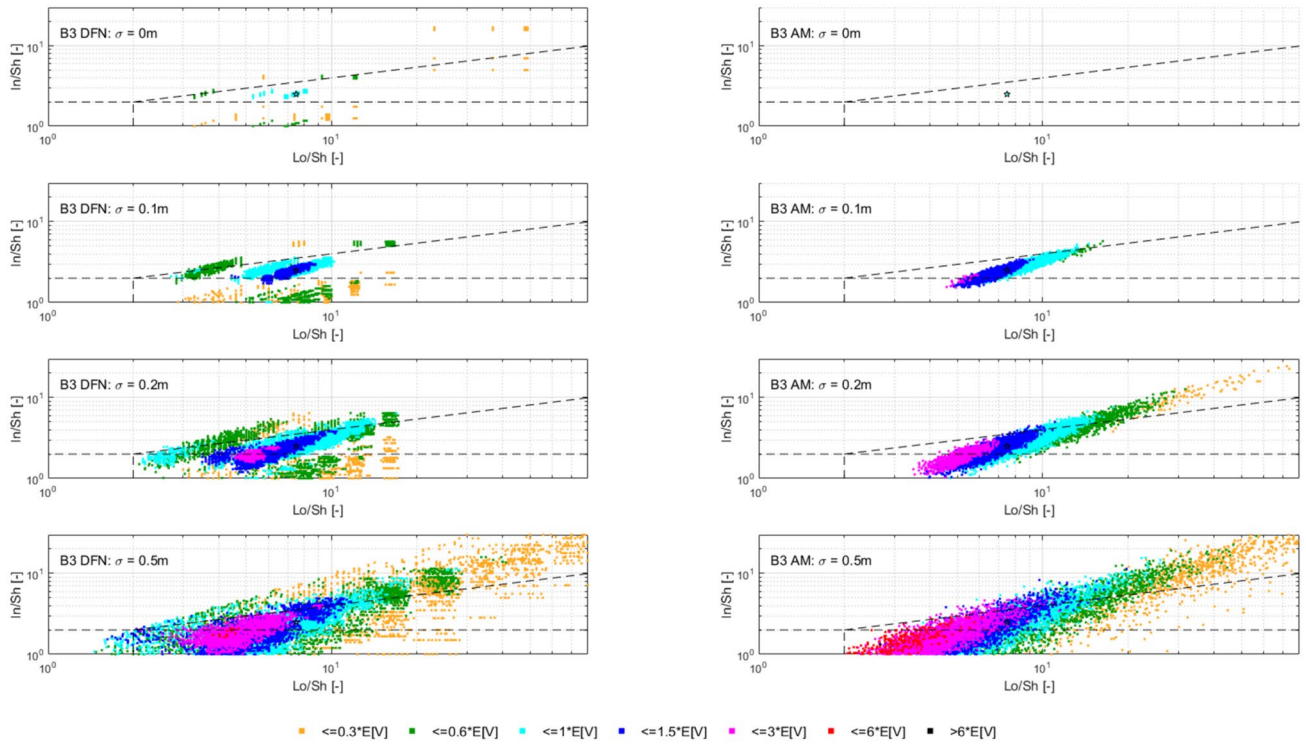

Fig. 9 Computed SDs in the case of reference block B3

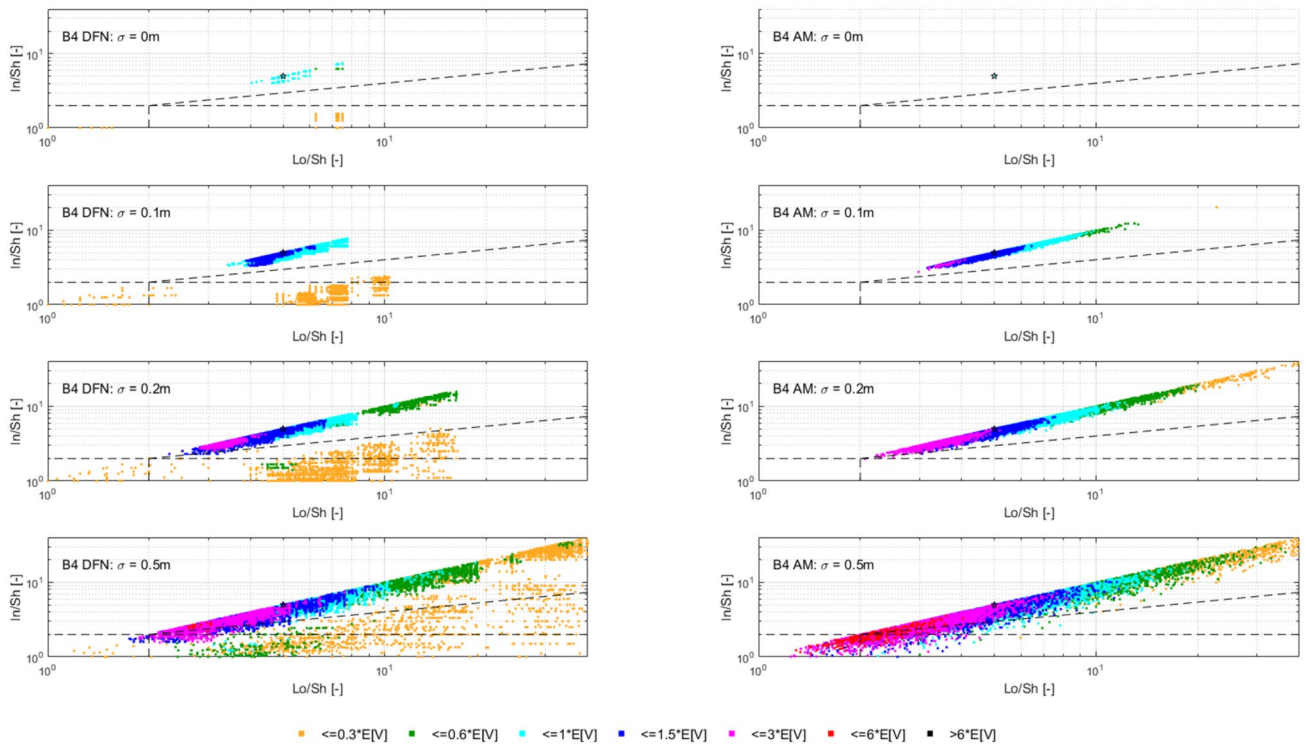

Fig. 10 Computed SDs in the case of reference block B4

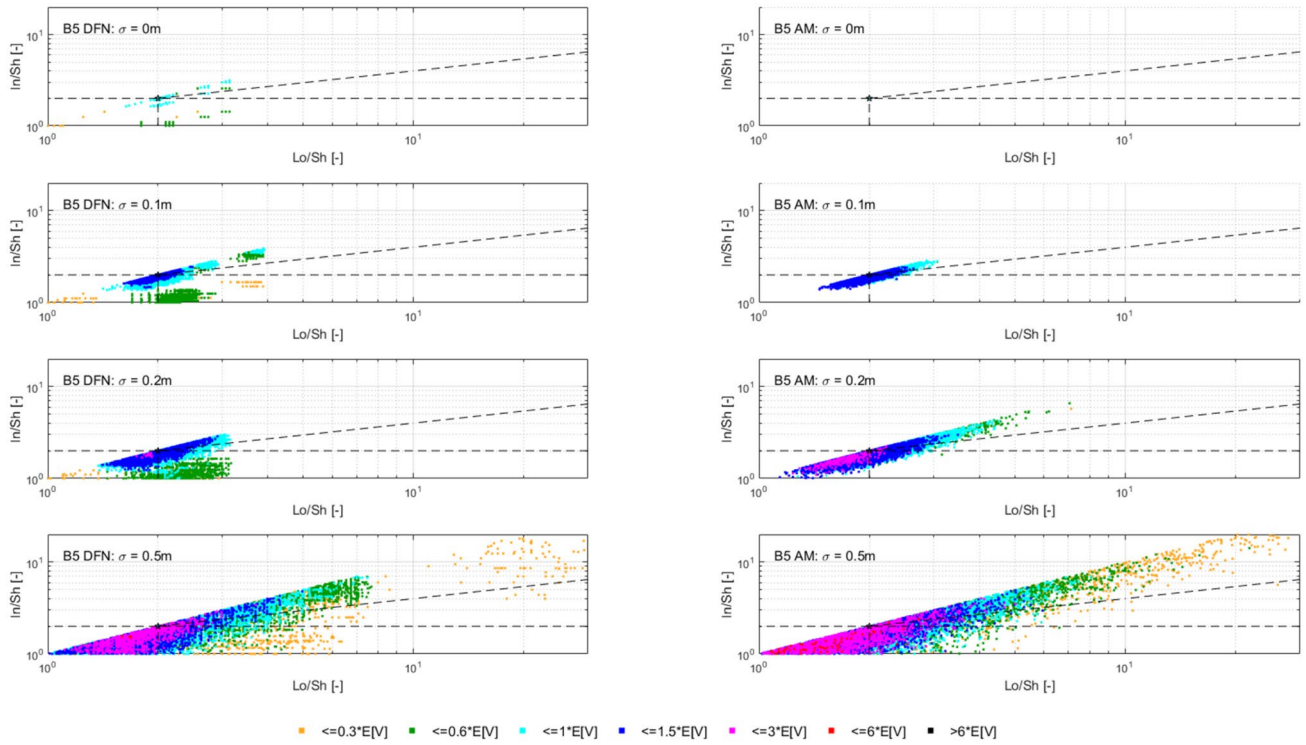

Fig. 11 Computed SDs in the case of reference block B5

4.2 Block Shape

Similar to what has been done for the IBSDs, Shape Distributions (SDs) have been separated according to the five reference block shapes shown in Fig. 6. Figures 7, 8, 9, 10, 11 portray Palmstrom's diagrams of blocks B1–B5, showing the effect of increasing σ value (from 0 to 0.5 m) for the parent spacing distributions.

The first noteworthy feature of these figures is the fact that as σ of the spacing distributions increases, the resulting blocks are plotted in an increasingly dispersed cloud stretching towards the right side of the diagram. Moreover, just as anticipated, if we distinguish the blocks based on their size (in our case, relative to the expected block size *E[V]*), it can be seen that the larger blocks (purple and red colored dots) tend to concentrate on the left side of the diagram. In the figures, this fact appears more clearly in the case of the AM-derived IBSDs, and is particularly evident in the case of block B3 (blade-like shape, Fig. 9). This is in part due to the issues with the way the DFN model is set up and its need for a pre-defined REV, as detailed in the previous Sect. 4. For such reasons, the size–shape distributions (SSDs) derived from the DFN model appear less homogeneously dispersed. Moreover, even in the case of $\sigma = 0$ for the spacing distributions, when the dot representing the single value SSD is expected to correspond directly with the reference point (the star in the diagrams), this condition is satisfied by all the AM-derived distributions, except for the B1 case (equidimensional shape), whilst the DFN derived distributions always show a degree of dispersion around the reference point. Again, this is a consequence of boundary effects along the pre-defined REV required to construct the DFN model. In this regard, it is clear that the AM-derived distributions, for both size and shape, appear to yield more consistent and reliable results.

These considerations regarding the effects of the DFN reliance on a pre-defined REV and boundary effects at the edges of the calculation volume can be extended to all the other cases described in Figs. 7, 8, 9, 10. In fact, by definition, a DFN analyzes only a pre-defined volume (i.e., the REV), considering it a model of the studied rock mass. Thus, the model size, although cautious and justified through quantitative means, as shown in this paper, still consists of a single, finite value. Therefore, the DFN-based approach appears intrinsically finite in nature, especially when compared to the AM, which does not require any model size but is purely based on the orientation and spacing distributions describing the joint sets. In other words, the AM describes the rock mass exclusively on a probabilistic level.

Alongside Palmstrom's diagrams, the easiest and clearest representation of an SD is a pie chart. In Figs. 12, 13, 14, 15, 16, two sets of pie charts are presented, describing the actual SD for each of the five reference shapes with increasing σ.

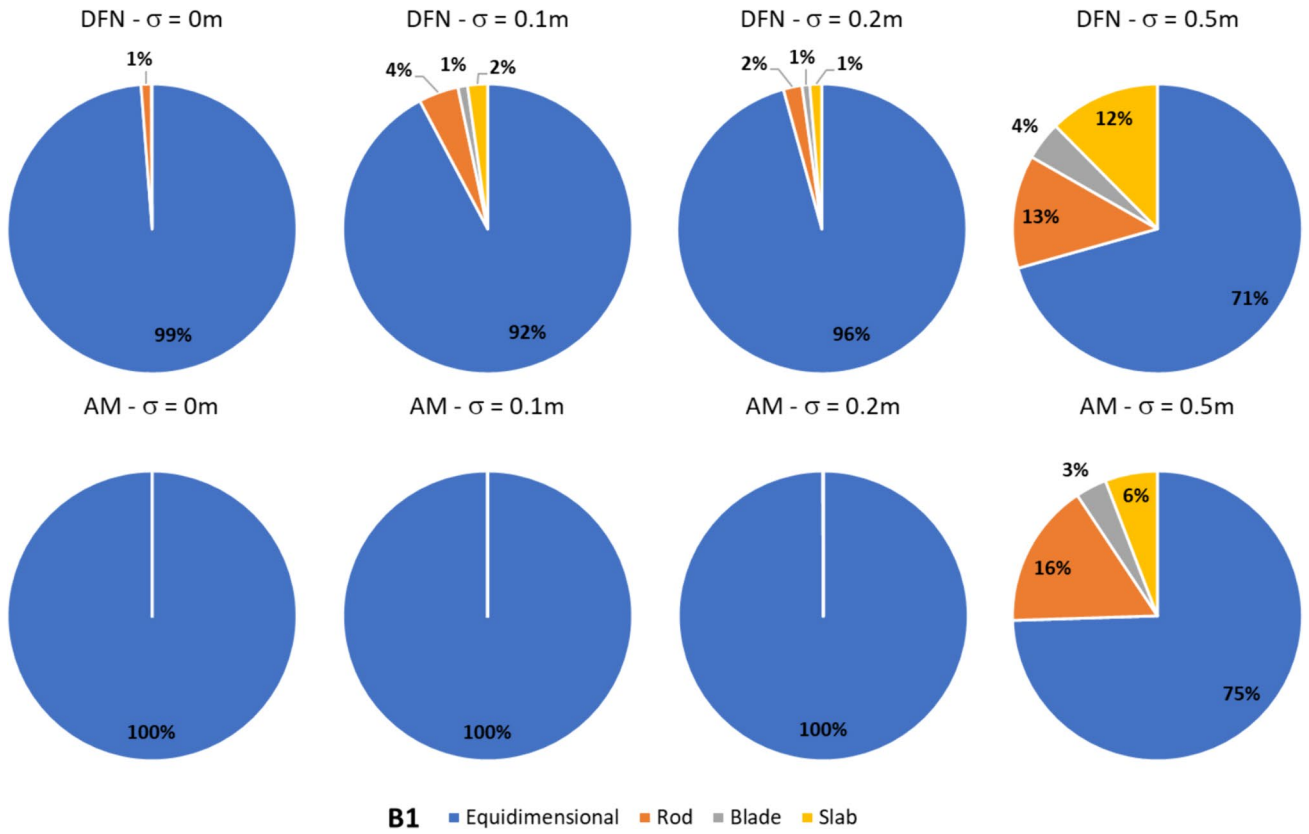

Fig. 12 Shape distribution pie charts for the B1 reference block

In Figs. 17, 18, 19, 20, 21, a second set describing the corresponding size distribution is presented.

A glance at the SD pie charts shows how similar the outputs of both methodologies are for high σ values (0.2 and 0.5 m) for the parent spacing distributions: in most cases, the difference between the DFN-derived and the AM-derived SDs are within a few percentage points. The results are significantly different among the two methods for low σ values (0 and 0.1 m): in almost all cases, the AM SD all show the expected shape as dominant, whilst the DFN SD allows for other shapes to appear, amounting to up to 16% of the distributions. The only exception is reference block B3 (blade-like block), where for σ = 0.1 m the AM SD, too, shows some variability in the possible shapes. This fact is, once again, related to the issues of the deterministic approach required by the DFN to work. Major differences are also found for reference block B4 (slab-like shape), where the AM SD describes the absence of non-slab-like blocks for cases with σ = 0, 0.1 and 0.2 m, whilst the DFN-derived SD states that non-slab-like blocks amount to approximately 15% (Fig. 15).

Considered here separately, for its specific and special nature, is reference block B5, which falls on the intersection of the shape domains within Palmstrom's diagram. This point describes a limit condition where none of the four classes upon which the shape classification is defined are applicable. Conversely, this point can be seen as sharing features of all the four classes, without belonging to one in particular. The special nature of this point is also linked to the fact that depending on the definitions of the boundaries between the four shape classes, one and only one set of conditions identifies the point. This means that the likelihood of a block appearing with this shape is extremely low, but more importantly, no other point outside of it can be classified in the same manner. Therefore, it is an especially interesting position to visualize the SSD (Figs. 16, 21).

Regarding the shape frequency pie charts (Fig. 16), apart from the case of σ = 0 m, the two methodologies produce very similar results: most of the larger blocks tend to fall clearly within the domain of equidimensional shapes. This is evident even in the case of the DFN-derived SSD: at σ = 0.5 m, the difference is approximately 1%. Regarding the volume distribution pie charts (Fig. 21), the special point B5 does not exhibit special features and behaves in accordance with all the others.

Looking at the second set of pie charts (Figs. 17, 18, 19, 20, 21), differences appear between the two methodologies. In general, the DFN-derived distributions tend to have a more significant number of blocks smaller than the expected

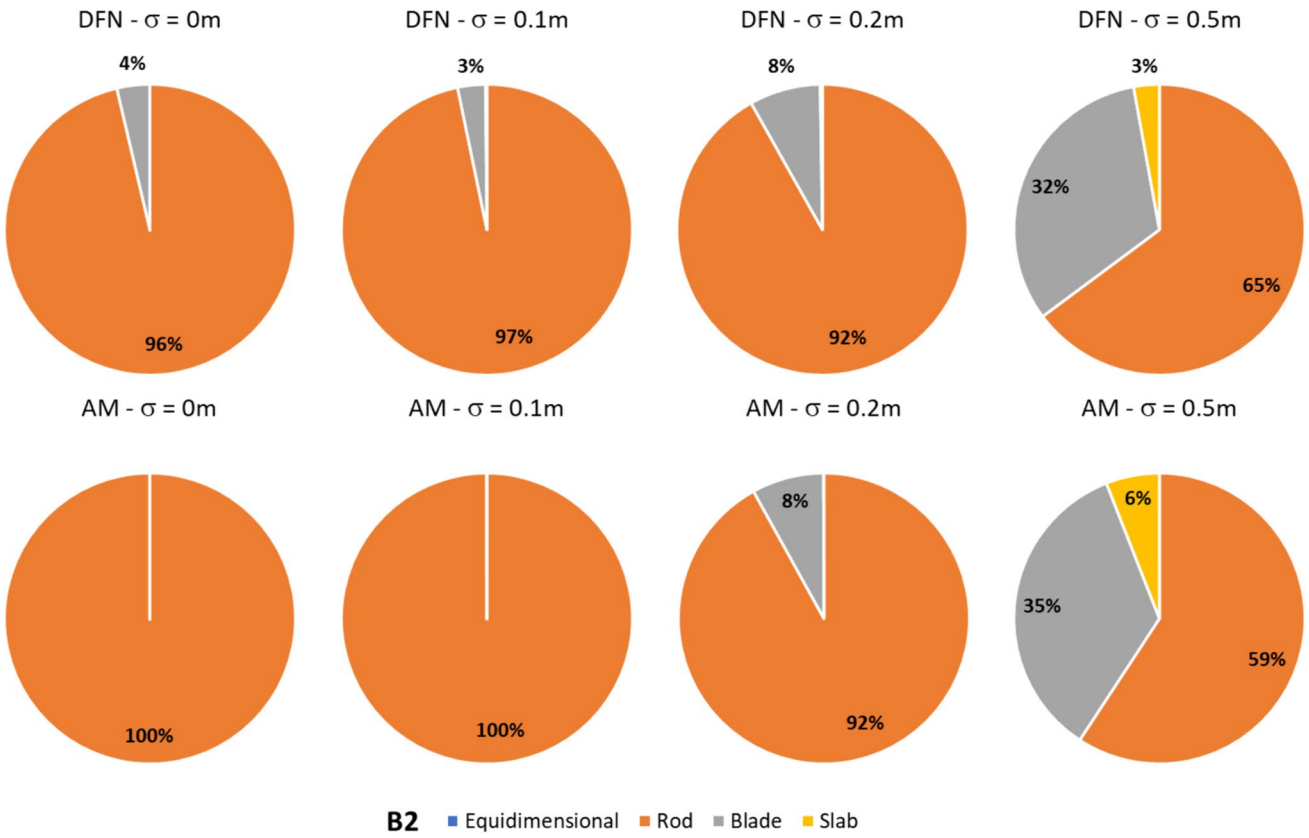

Fig. 13 Shape distribution pie charts for the B2 reference block

block size ($V < 1\ E[V]$) and usually miss entirely the largest ones ($V > 6\ E[V]$). As σ of the parent spacing distributions increases, the dispersion of the size data throughout the considered classes increases, and the differences between the two methods tend to reduce. In fact, for $\sigma = 0.5$ m, the distributions are significantly close to each other, taking into account the tendency of the DFN data to have a higher count of smaller blocks. For instance, in the case of reference block B1 (equidimensional shape, Fig. 17), most of the computed blocks fall within 1 $E[V]$ and 1.5 $E[V]$, with remarkably similar percentages for both approaches: for 1 $E[V]$, 32% in the case of the DFN derived data, 33% for the AM; for 1.5 $E[V]$, 26% and 28%, respectively. It should be noted that the issues of the DFN model are the same discussed in the paragraph on block size (Sect. 4.2): boundary issues introduce artificially smaller blocks and impose an upper limit to block size.

4.3 Case Study

To show an application of what has been introduced in the previous paragraphs regarding the block size–shape relationship, a case study has been selected. In Taboni et al. (2023), the rockfall hazard assessment of the site of Grangia Cruset (Municipality of Bellino, Province of Cuneo, Piemonte Region) is presented. Located in the westernmost portion of Varaita Valley, in the Western Italian Alps, the exposed buildings are located at the toe of a steep slope overhung by rocky peaks, which act as rockfall sources. The most recent event was registered in 2017 and involved a total volume of approximately 100 m^3 of fallen rocks, estimated by measuring the scar left on the rockface. Most of the blocks that actually reached the exposed buildings had a volume of approximately 1 m^3, while the largest single boulder reached 6 m^3. No data are available on the number or volume of the originally detached blocks: although no evidence of fragmentation was found, it is not impossible that during the rockfall the original blocks experienced it. Thus, as the referenced data describe the blocks measured after the event and at their stopping position, their size represents a lower bound on the initially released block sizes. Thus, the possible fragmentation of larger volumes was not considered. The authors produced a new methodology for rockfall hazard assessment, employing IBSD to describe block size and an SD for its shape; they then ran four sets of one thousand 3D simulations of block trajectories, one for each of the four shape types defined by Palmstrom (2001), and integrated the result for a global description of the problem. The SD used was referred to the entire IBSD, which may differ

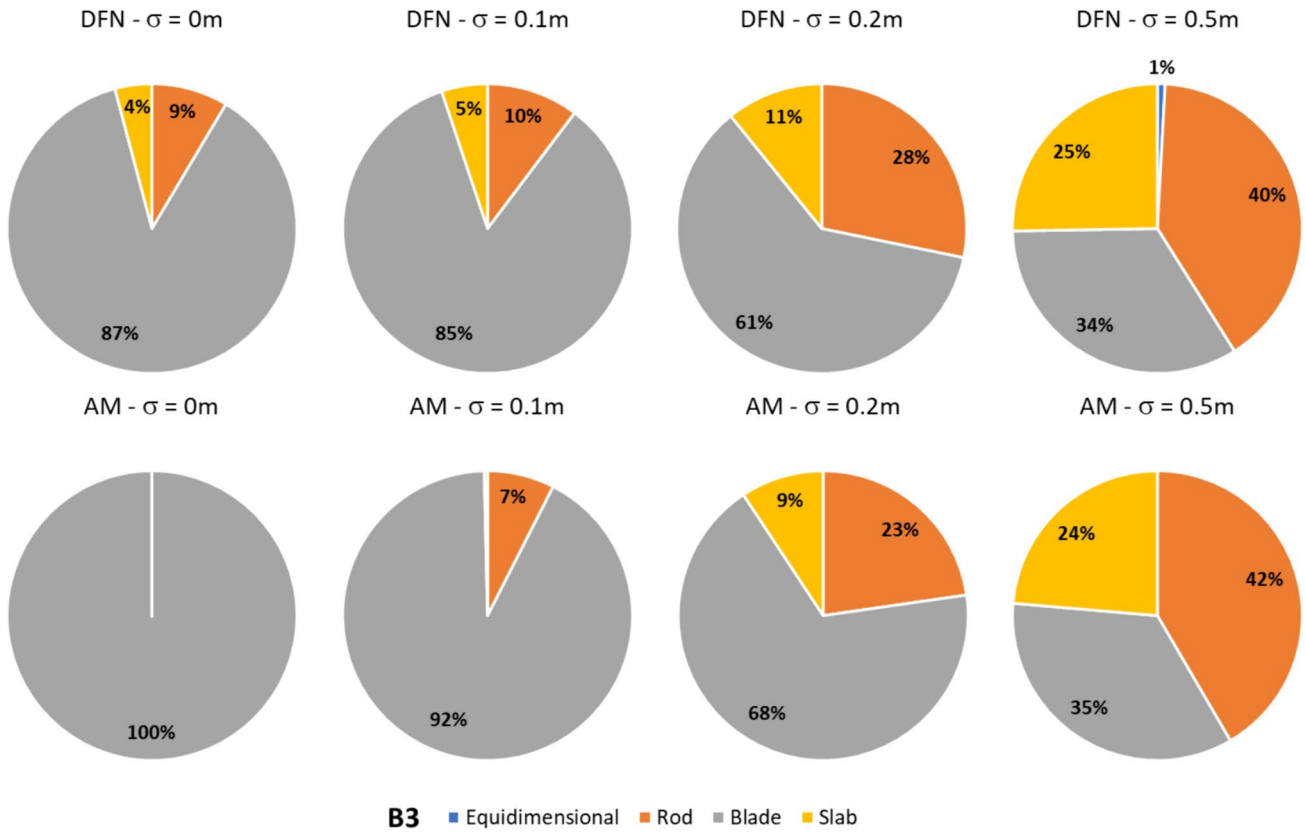

Fig. 14 Shape distribution pie charts for the B3 reference block

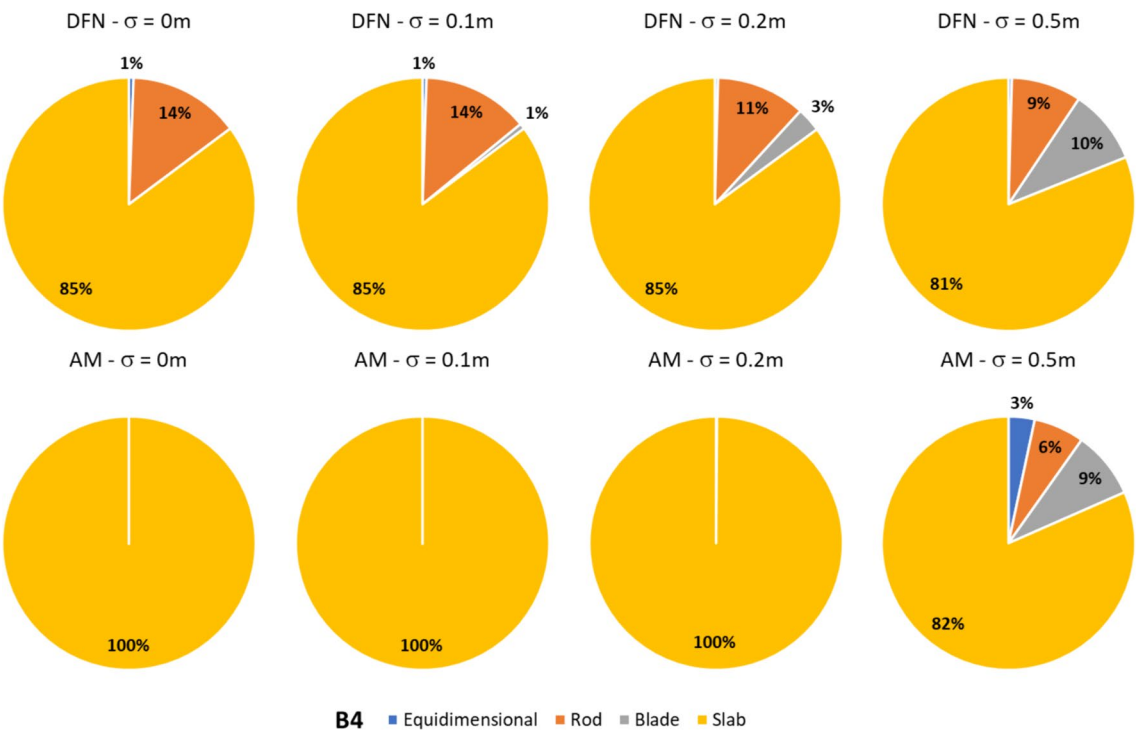

Fig. 15 Shape distribution pie charts for the B4 reference block

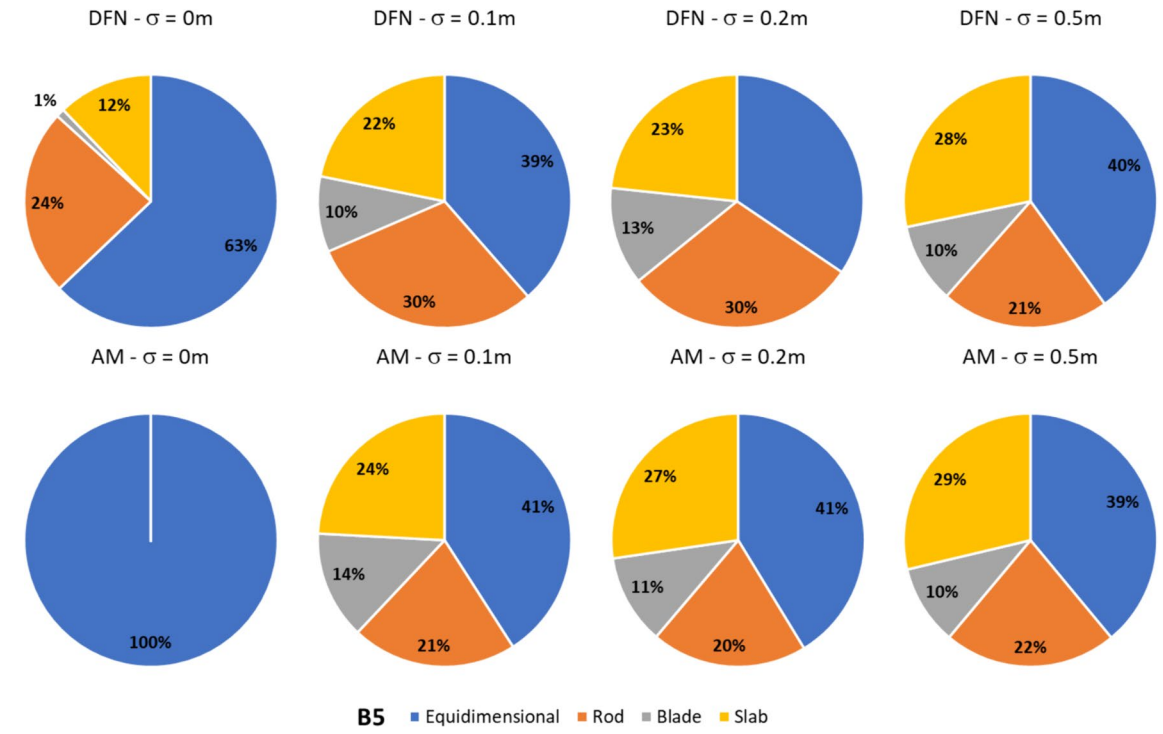

Fig. 16 Shape distribution pie charts for the B5 reference block

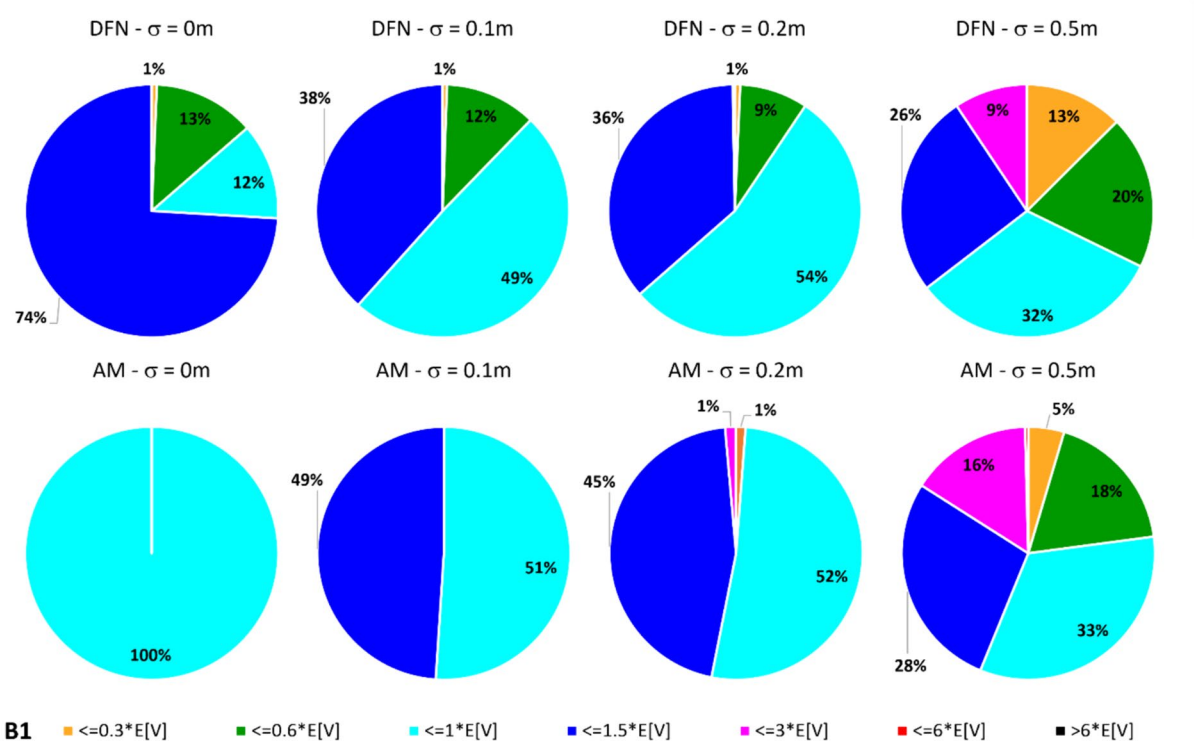

Fig. 17 Pie charts describing block size for reference block B1

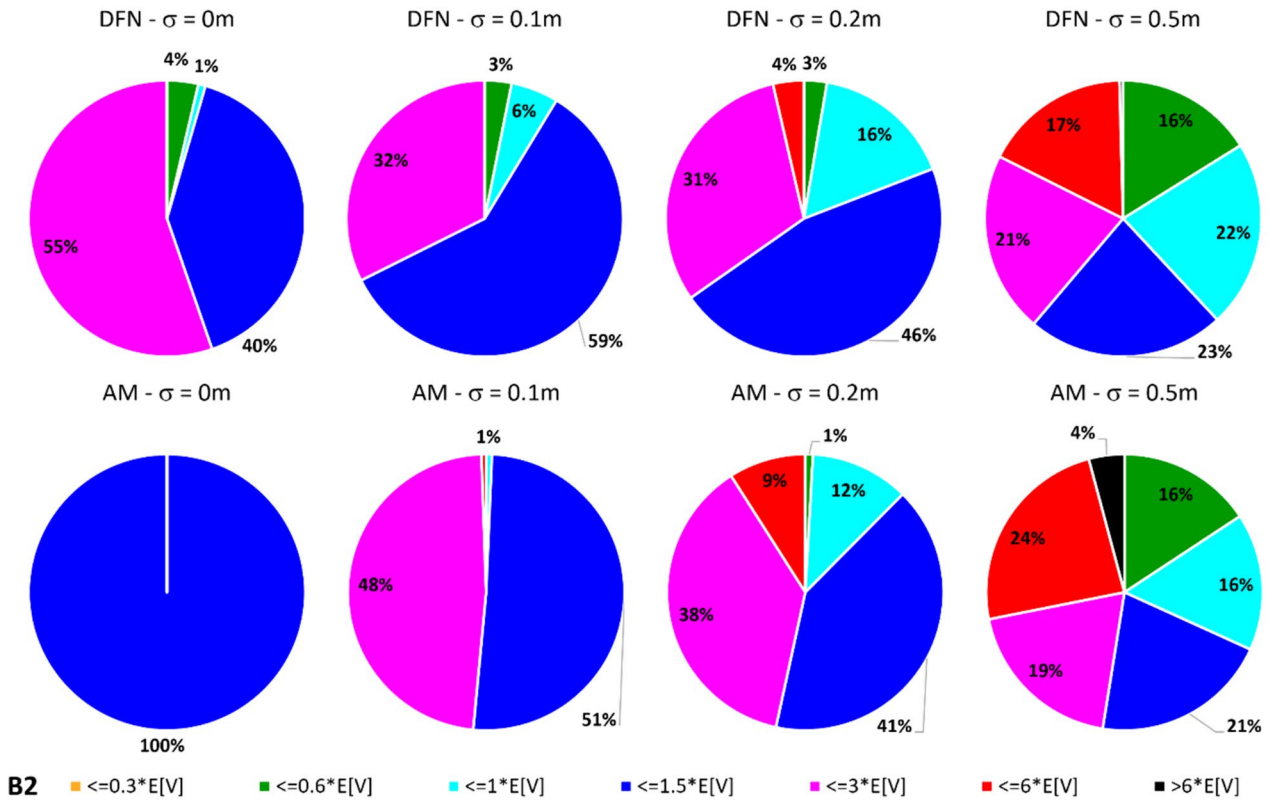

Fig. 18 Pie charts describing block size for reference block B2

significantly as the volume increases, as it was shown in the previous paragraphs. Thus, as the relationship between block size and volume was not addressed in the original paper, the same case study can be used to provide a quick but reliable example of how to implement it in a real situation without increasing complexity at the point of making the methodology impractical and, thus, useless. It should be mentioned that only the AM was employed for the case study at hand.

For the purpose of this study, the same IBSD and SD described in Taboni et al. (2023) are considered: they are reported in Table 5. To properly integrate the size–shape correlation into the rockfall numerical analysis, the approach consists of filtering out the shapes of the SD belonging to rock blocks whose volumes fall out of a given interval. A reasonable interval can be derived from the existing regulations regarding passive rockfall mitigation works, which usually insist upon incrementing the reference design volume by applying a partial factor (UNI 11211 2019) to account for a higher effect of the acting force, namely the kinetic energy of the impacting block. For this reason, we chose to filter the SD within a range of ± 10% of the reference volume, which was estimated to be 6.5 m^3 (slightly larger than the largest block recorded on site, amounting to 6 m^3). To assess the effect of size–shape correlation on smaller blocks, the average registered block (1 m^3) was also modeled. By filtering out all the blocks that fall out of the interval, the resulting filtered SD now describes only the relative abundances of the shapes associated with blocks comparable to the reference volume; therefore, the filtered SD provides a more accurate shape sample.

Finally, following the same workflow of the original paper, new global results for the 3D numerical simulations based on the filtered SDs were produced by calculating, as suggested by Taboni et al. (2023), and average weighted over the relative abundances of the four shape classes, according to the following relation:

$$\mathrm{SO} = \left(\mathrm{PO}_e \cdot e\right) + \left(\mathrm{PO}_r \cdot r\right) + \left(\mathrm{PO}_s \cdot s\right) + \left(\mathrm{PO}_b \cdot b\right), \quad (9)$$

where *SO* is the global output; PO_e, PO_r, PO_s, and PO_b are the partial output for the equidimensional, rod-like, slab-like, and blade-like shape, respectively; *e*, *r*, *s* and *b* are the relative abundance of the equidimensional, rod-like, slab-like, and blade-like shapes within the considered SD.

The Grangia Cruset case study presented by Taboni et al. (2023) has been modified and integrated to account for the shape–size correlation. The IBSD employed in the original paper has been filtered out, extracting two different portions:

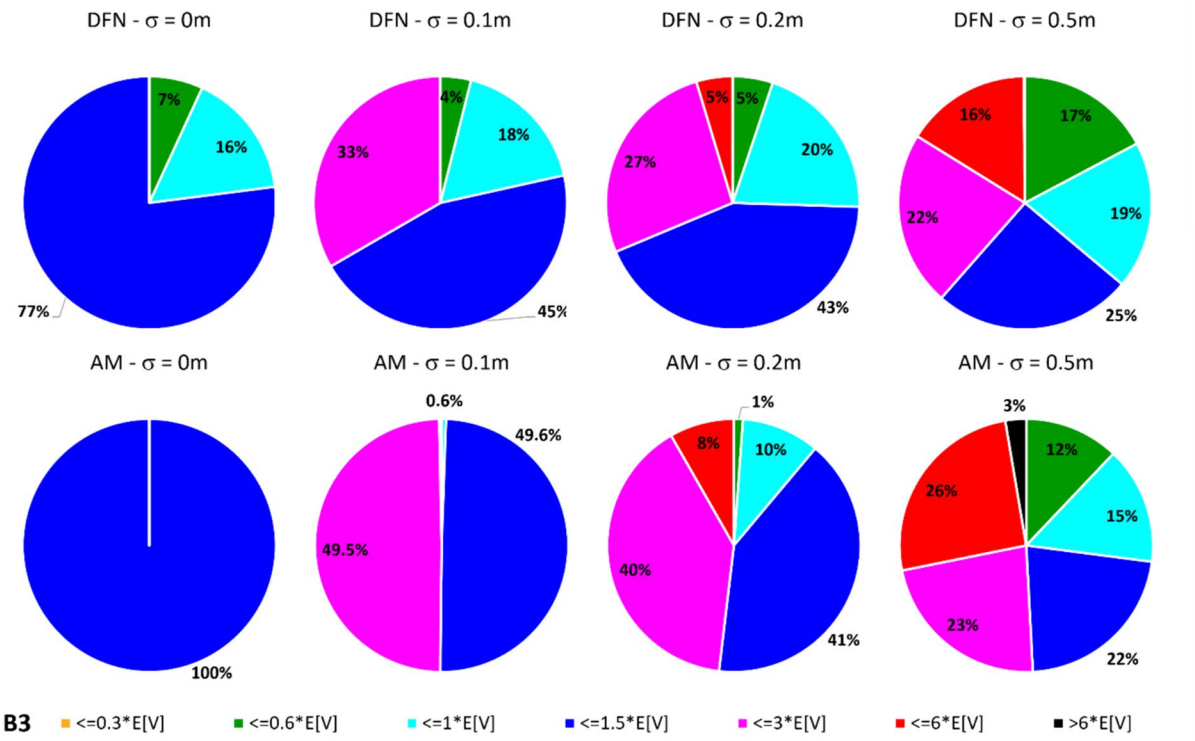

Fig. 19 Pie charts describing block size for reference block B3

the one within a 10% range around the reference design value (6.5 m^3) and the one within a 10% range around the average recorded falling block (1 m^3); then, the two new SDs have been computed and new numerical simulations carried out. The slope model is exactly the same as the original paper. From here onward, the same methodology detailed in Taboni et al. (2023) has been followed to combine the contributions of each of the four shapes. Figure 22 shows the comparison between the original global SD and the new ones, focused on the two considered block sizes.

As it can be seen, the difference is significant: for instance, in the 6.5 m^3 case, equidimensional blocks are more relevant (+ 12%) than in the global SD, while rod-like blocks are less frequent (−14%); meanwhile, for the 1 m^3 case, equidimensional blocks are less frequent (−7%), alongside blade-like blocks (−10%), whilst slab-like blocks appear to be more prominent (+ 12%). Once again, the increase of equidimensional blocks at higher volumes, or conversely, their decrease at lower volumes, is appreciable. The effect of the new SDs on the maps produced by the 3D rockfall software Rockyfor3D (Dorren 2016) is difficult to appreciate based solely on the maps themselves. To quantify the difference, data regarding total kinetic energy (E_k) have been extracted along a line, symbolizing the extent of a possible protection work. Figure 23 describes the case for the 6.5 m^3 block, while the Fig. 24 compares the E_k values of the original run of simulations and the new one along that line.

As can be seen, the energy involved in a rockfall event for a 6.5 m^3 block is consistently lower if the filtered SD is considered. On average, the difference is between 5 and 10% of the original value (between 1000 and 2000 kJ). Unfortunately, considering that the reference energy level of the modeled phenomenon, as stated in the original paper, is in the range of 25,000 kJ, a difference of 10% does not significantly affect the design process of any kind of protection work. A similar trend can be observed also for the bounce height. Figures 24 and 25 present the results for the 1 m^3 case.

While in the previous case, the new set of simulations produced lower E_k outputs, and the difference is between 10 and 20%, in this second instance, the new values are actually higher than the original outputs. More importantly, as the maximum energy value extracted is close to 5000 kJ, a difference of 1000 kJ signifies a skip between different commercial classes of passive protection works, such as flexible barriers. This is important, as commercial rockfall barriers are sold in pre-defined energy categories: for example, if referencing the original outputs, a 5000 kJ barrier would have been enough, while for the new results, a higher energy level is required. Usually, this means employing an 8000 kJ kit, with a significant increase in the costs.

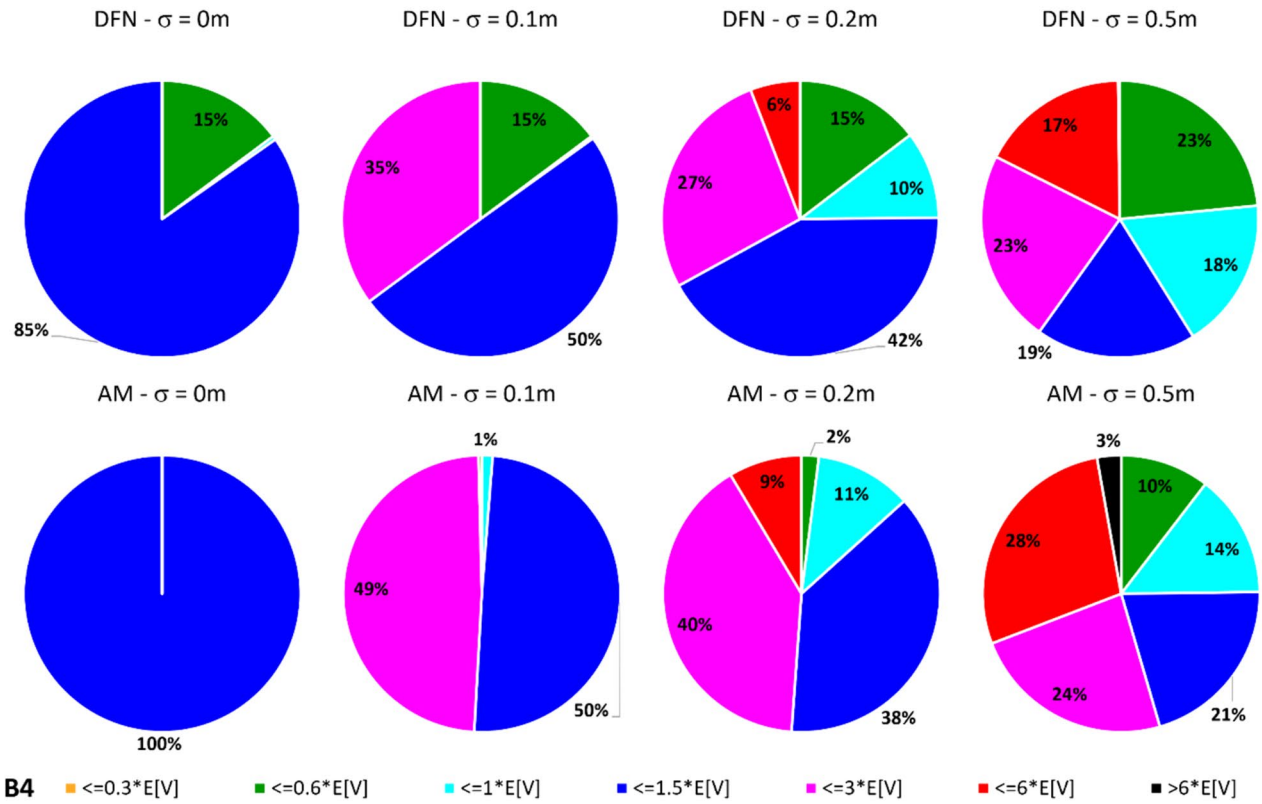

Fig. 20 Pie charts describing block size for reference block B4

The fact that in both Figs. 24 and 26, the new model appears very similar to the original one, simply shifted towards higher or lower energy levels, is not to be intended in any way as a feature of the approach presented here. This fact is likely due to two aspects: first and foremost, the configuration of the model (i.e., the topography and the features of the slope) is the same in both simulations; second, the case study manifests an apparent propensity to concentrate almost all the trajectories along the paths highlighted in Figs. 23 and 25. By filtering the SD around the reference block sizes, the achieved effect is akin to extracting a precise portion of the simulated blocks from the more generalized original set of simulations. This is to say that the new results being similar to the original ones are, at least in this specific case, to be expected.

In general, therefore, two things can be said: first, accounting for the Shape–Size correlation could produce tangible effects on the modeling of the rockfall process; second, mass, and thus block size, seems to have a more relevant role, as for larger blocks the difference in the computed values decreases and is less relevant.

5 Conclusions

The present work aims to compare the DFN-based and the AM-based approaches to the characterization of rock masses geometrical structure for rockfall assessment purposes. These two methods are based on different assumptions and different calculation algorithms. On the one hand, a DFN is able to generate a virtual model of the rock mass by cutting the defined box along input planes representing discontinuities. Therefore, blocks volume and side lengths are outputs of the modeling process, which requires the assessment of the REV to reduce the boundary effect. On the other hand, the proposed AM-based approach is a purely analytical method, incapable of materializing and modeling the rock mass structure, but able to calculate an IBSD based on its analytical definition, without the need to assess a REV. In conclusion, it was seen that both approaches are viable when dealing with:

– Block size assessment, although the DFN-based methodology has some intrinsic limitations (boundary effects on smaller blocks; upper size limit) that may hinder the accuracy of the outputs in some specific circumstances (low σ of the parent spacing distributions). The DFN-

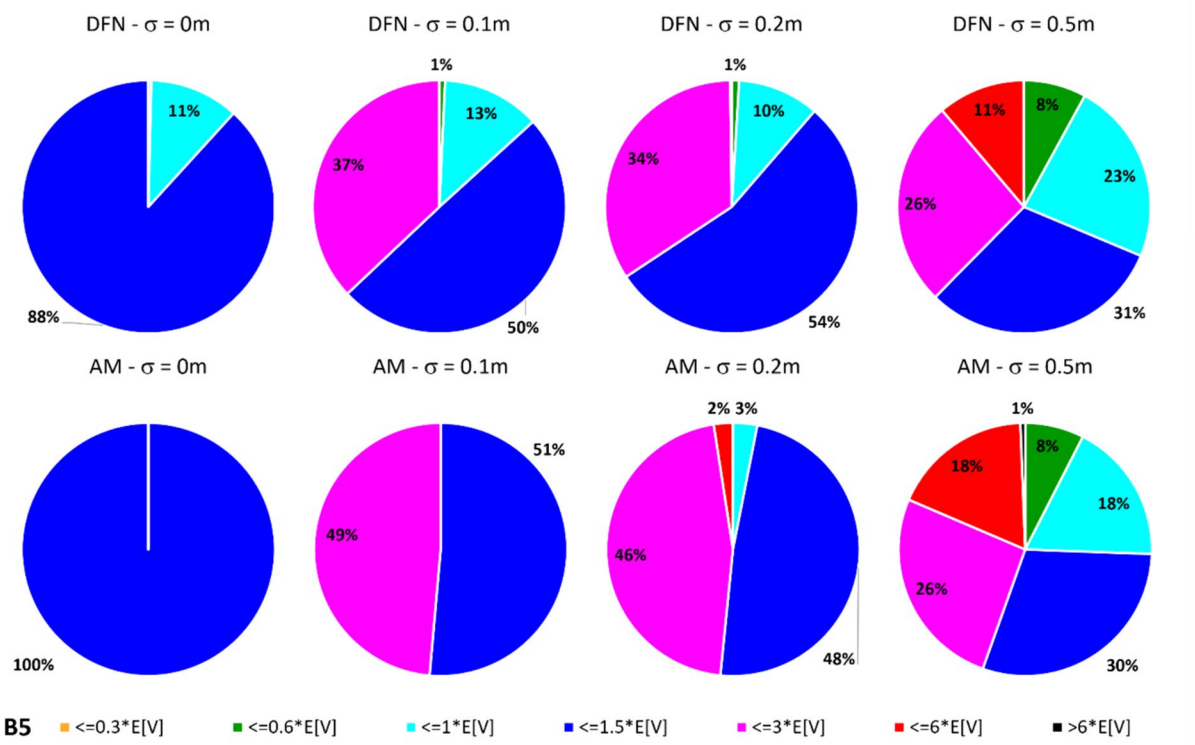

Fig. 21 Pie charts describing block size for reference block B5

Table 5 Parameters of the best-fitting distributions of spacing samples for the three joint sets identified in the case study analyzed by Taboni et al. (2023)

K1			K2			K3		
PDF	μ_1 [m]	σ_1^2 [m^2]	PDF	μ_2 [m]	σ_2^2 [m^2]	PDF	μ_3 [m]	σ_3^2 [m^2]
LogNormal	2.21	7.69	Weibull	1.91	2.48	Weibull	1.69	1.30

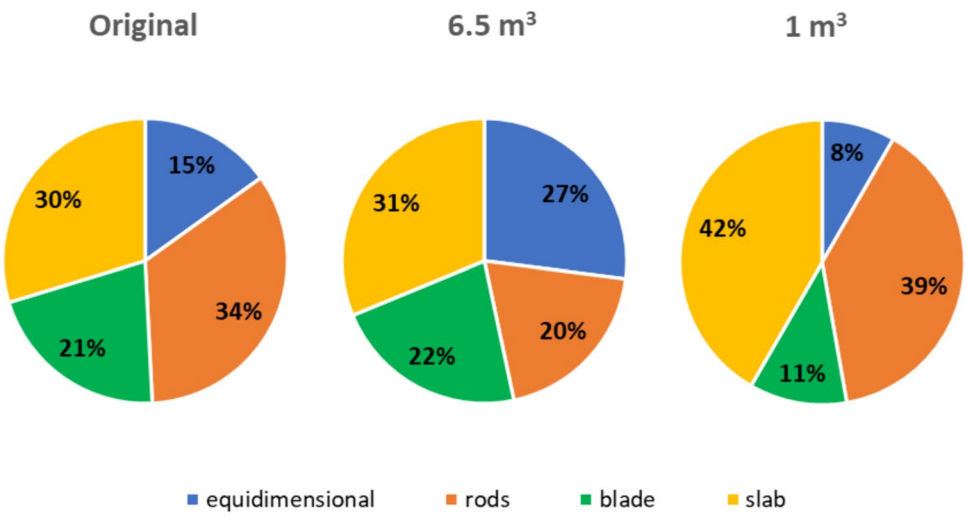

Fig. 22 SDs for the Bellino case study: the original SD (left) (from Taboni et al. 2023), the SD focused on the 6.5 m^3 block (middle), and the SD focused on the 1 m^3 block (right)

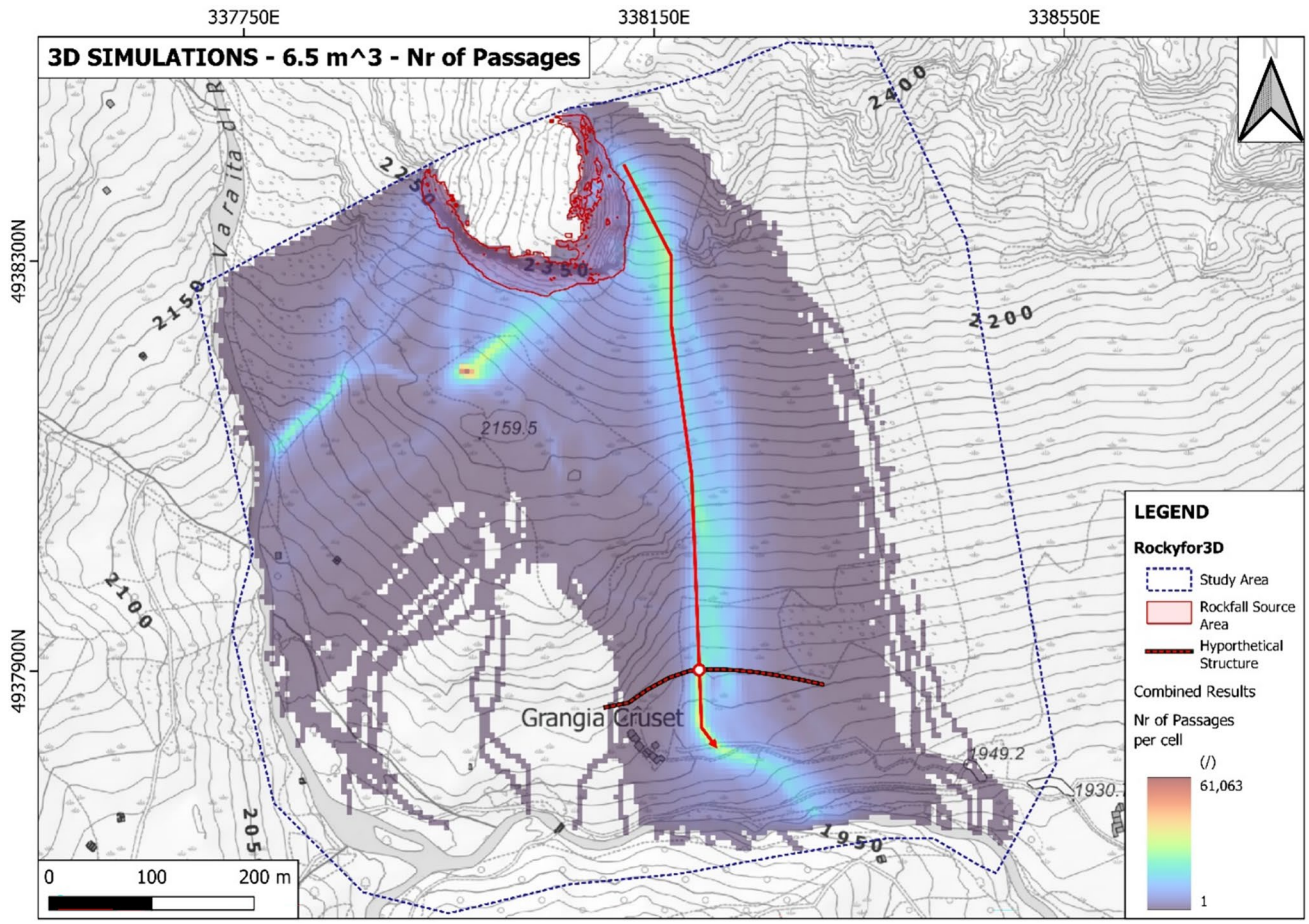

Fig. 23 Runout model for the 6.5 m^3 case, with the most frequent path in red and the trace of a hypothetical protection work

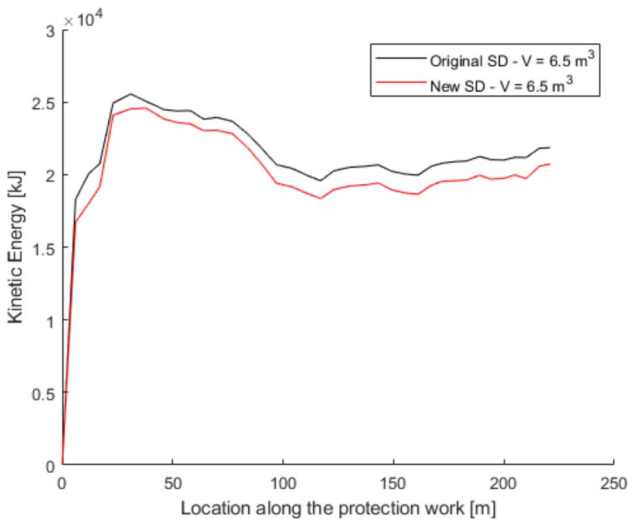

Fig. 24 Comparison between E_k of the original (black line) and new 6.5 m^3 simulations (red line) along the hypothetical protection work

based approach has no issues in dealing with instances where more than three joint sets are identifiable, while the analytic one would require a combinatory application of the method; finally, the analytic method can handle different types of PDF without particular issues, but in the case of rock masses characterized by more than three joint sets, the approach cannot be directly employed, rendering it, in that specific case, less flexible than a DFN. Both approaches yield consistently similar and comparable results.

– Block shape assessment, although the basic assumptions of the DFN-based method tend to produce more clustered outputs for low σ of parent spacing distributions.

Moreover, both methodologies identify the existence of a correlation between shape and size of the computed blocks, which dictates that the SD changes with reference to block size. The method to assess such correlation, as well as the way to implement it in rockfall numerical simulations or hazard assessment shown in this study, can easily be applied to both DFN-derived and AM-derived data.

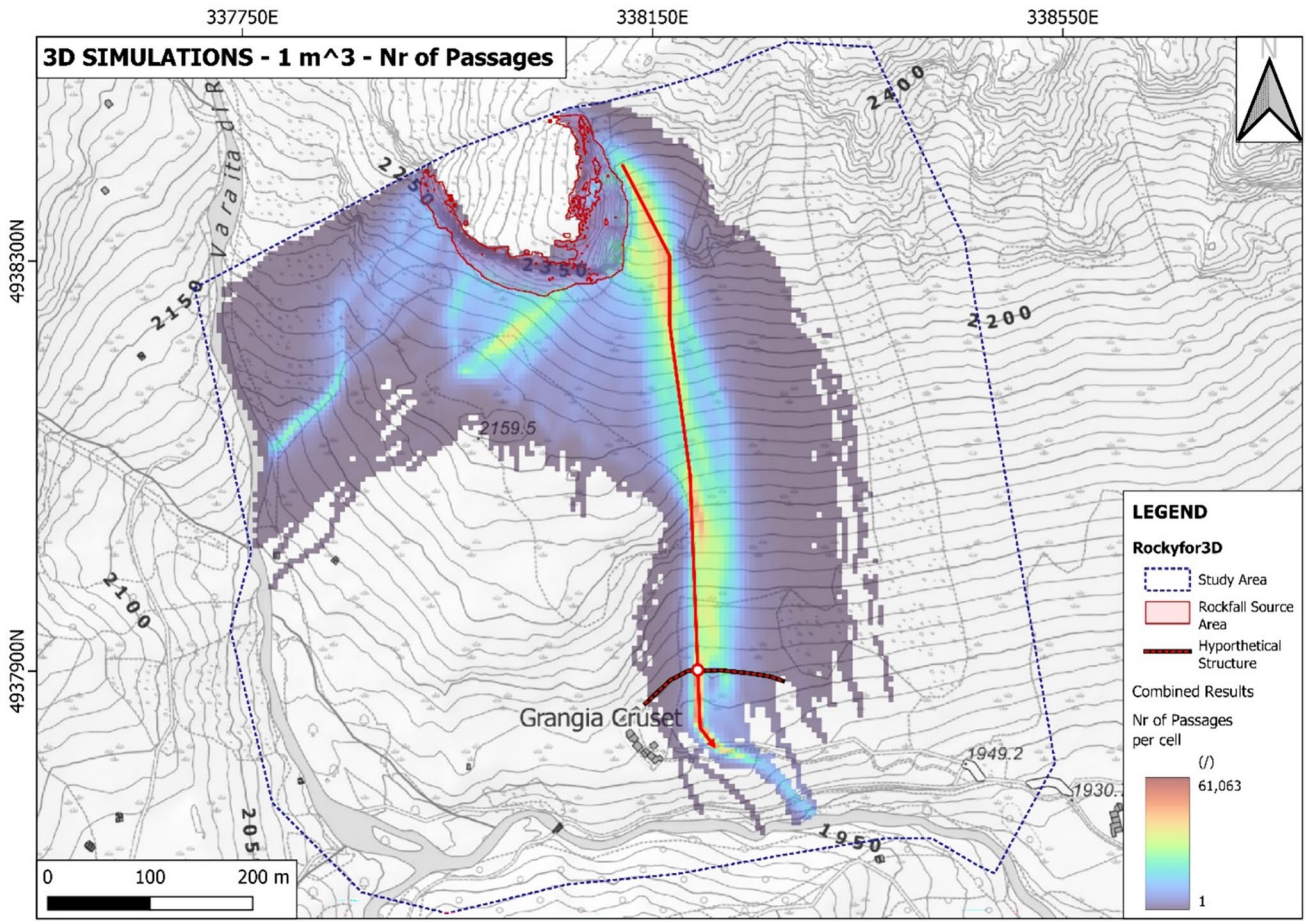

Fig. 25 Runout model for the 1 m^3 case, with the most frequent path in red and the trace of a hypothetical protection work

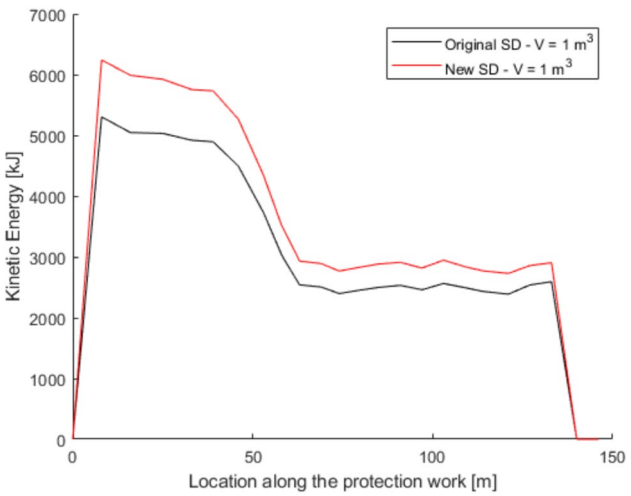

Fig. 26 Comparison between E_k of the original (black line) and new 1.0 m^3 simulations (red line) along the hypnotized protection work

The case study allowed us to visualize and quantify the differences that arise when accounting for the shape–size correlation. Moreover, it demonstrated that size plays a more significant role, as in the case of larger blocks, the effects of a quite different SD are less relevant than in the case of a smaller block.

It is crucial to notice that two important questions remain open. First of all, the actual appearance of an IBSD, its corresponding SD, and the correlation between the two are derived from safe and reasonable assumptions (Umili et al. 2023) and have yielded accurate and reliable results. Further studies are required to demonstrate such assumptions and the considerations derived from them.

The information provided by modeling the geometric features of a rock mass, either by means of DFNs or analytical methods, is critical to properly constructing a model for numerical simulations of the phenomenon. Thus, it is highly important for practitioners and designers, who directly rely on the output of such simulations to acquire the needed data required to design protection structures or other mitigation measures correctly. This is also true

for land planners, as numerical simulations are usually involved in hazard and risk assessment and mapping. Both block size and block shape are highly relevant parameters for rockfall, which yield direct influences on the outcomes of the simulations. This is especially significant given the now widespread presence of software based on the rigid body approach to rockfall, which are able to account for both rock size and shape.

Being able to produce more precise and accurate models from a reliable input dataset, rigorously produced through a solid and repeatable methodology, is a significant improvement across all fields of application.

Funding Open access funding provided by Università degli Studi di Torino within the CRUI-CARE Agreement. This research did not receive any specific grant from funding agencies in the public, commercial, or not-for-profit sectors.

Declarations

Conflict of interest The authors have no relevant financial or non-financial interests to disclose.

References

Andersson J, Shapiro AM, Bear J (1984) A stochastic model of a fractured rock conditioned by measured information. Water Resour Res 20(1):79–88

Baecher GB (1983) Statistical analysis of rock mass fracturing. J Int Assoc Math Geol 15(2):329–348

Bhusan R, Naik SR, Sekar V (2020) Support assessment and 3D stress analysis of large underground excavations: a case study using 3DEC. In: Billaux, Hazzard, Nelson, Schöpfer (eds) Applied numerical modeling in geomechanics, Paper: 01–05. Itasca International Inc., Minneapolis

Bourrier F, Acary V (2022) Predictive capabilities of 2D and 3D block propagation models integrating block shape assessed from field experiments. Rock Mech Rock Eng 55(2):591–609. https://doi.org/10.1007/s00603-021-02696-5

Buyer A, Aichinger S, Schubert W (2020) Applying photogrammetry and semi-automated joint mapping for rock mass characterization. Eng Geol 264:105332. https://doi.org/10.1016/j.enggeo.2019.105332

Caviezel A, Ringenbach A, Demmel S, Dinneen C, Krebs N, Buhler Y, Christen M, Meyrat G, Stoffel A, Hafner E, Eberhard L, Reckenbach D, Simmler K, Mayer P, Niklaus P, Birchler T, Aebi T, Cavigelli L, Schaffner M, Rickli S, Schnetzler C, Magno M, Benini L, Bartelt P (2021) The relevance of rock shape over mass—implications for rockdall hazard assessments. Nat Commun 12:1. https://doi.org/10.1038/s41467-021-25794-y

Dershowitz WS, Einstein HH (1988) Characterizing rock joint geometry with joint system models. Rock Mech Rock Engng 21:21–51. https://doi.org/10.1007/BF01019674

Dorren LKA (2016) Rockyfor3D (v5.2) Revealed—transparent description of the complete 3D rockfall model. ecorisQ paper (www.ecorisq.org), p 32

Esmaieli K, Hadjigeorgiou J, Grenon M (2010) 2010. Estimating geometrical and mechanical REV based on synthetic rock mass models at Brunswick mine. Int J Rock Mech Min Sci 47(6):915–926. https://doi.org/10.1016/j.ijrmms.2010.05.010

Fan H, Li L, Zong P, Liu H, Yang L, Wang J, Yan P, Sun S (2023) Advanced stability analysis method for tunnel face in jointed rock masses based on DFN-DEM. Undergr Space 13:136–149. https://doi.org/10.1016/j.undsp.2023.03.009

Feng X, Li D, Wang L, Jing Y, Xun X, Zeng Q (2011) A new method of block shape classification. Sci China Tech Sci 54:110–115. https://doi.org/10.1007/s11431-010-4221-z

Hudson JA, Harrison JP (1997) Engineering rock mechanics. Elsevier, Oxford

Huang X, Li S, Jin J, Shi C (2024) Determining digital representation and representative elementary volume size of broken rock mass using the discrete fracture network-discrete element method coupling technique. Appl Sci 14:606. https://doi.org/10.3390/app14020606

ITASCA (2007) 3DEC (3 dimensional distinct element code) version 4.1. Itasca Consulting Group Inc., Minneapolis

Kalenchuk KS, Diederichs MS, McKinnon S (2006) Characterizing block geometry in jointed rockmasses. Int J Rock Mech Min Sci 43(8):1212–1225. https://doi.org/10.1016/j.ijrmms.2006.04.004

Kalenchuk KS, McKinnon S, Diederichs MS (2008) Block geometry and rockmass characterization for prediction of dilution potential into sub-level cave mine voids. Int J Rock Mech Min Sci 45(6):929–940. https://doi.org/10.1016/J.IJRMMS.2007.10.006

Kobayashi Y, Harp EL, Kagawa T (1990) Simulation of rockfalls triggered by earthquakes. Rock Mech Rock Eng 23:1–20

Kong D, Wu F, Saroglou C, Sha P, Li B (2021) In-situ block characterization of jointed rock exposures based on a 3D point cloud model. Remote Sens 13:2540. https://doi.org/10.3390/rs13132540

Koulibaly AS, Shahbazi A, Saeidi A, Rouleau A, Quirion M, Chesnau R (2023) Advancements in rock block volume calculation by analytical method for geological engineering applications. Env Earth Sci 82:344. https://doi.org/10.1007/s12665-023-11027-6

Leine RI, Capobianco G, Bartelt P, Christen M, Caviezel A (2021) Stability of rigid body motion through an extended intermediate axis theorem: application to rockfall simulation. Multibody Syst Dyn 52:431–455. https://doi.org/10.1007/s11044-021-09792-y

Leine RI, Schweizer A, Christen M, Glover J, Bartelt P, Gerber W (2014) Simulation of rockfall trajectories with consideration of rock shape. Multibody Syst Dyn 32:241–271. https://doi.org/10.1007/S11044-013-9393-4

Lu P, Latham J-P (1999) Developments in the assessment of in-situ block size distributions of rock masses. Rock Mech Rock Eng 32:29–49. https://doi.org/10.1007/s006030050042

Mauldon A (1994) Intersection probabilities of impersistent joints. Int J Rock Mech Min Sci 31(2):107–115. https://doi.org/10.1016/0148-9062(94)92800-2

Noël F, Cloutier C, Jaboyedoff M, Locat J (2021) Impact-detection algorithm that uses point clouds as topographic inputs for 3D rockfall simulations. Geosciences 11(5):188. https://doi.org/10.3390/geosciences11050188

Noël F, Cloutier C, Turmel D, Locat J (2016) Using point clouds as topography input for 3D rockfall modeling. Landslides and

Engineered Slopes. Experience, Theory and Practice. CRC Press, Napoli, pp 1531–1535. https://doi.org/10.1201/9781315375007-178

Palmstrøm A (2001) Measurement and characterization of rock mass jointing. In: Sharma VM, Saxena KR (eds) In-situ characterization of rocks. Balkema, Rotterdam, pp 49–97

Pfeiffer T, Bowen T (1989) Computer simulation of rockfalls. Bull Assoc Eng Geol 26:135–145

Singh J, Pradhan SP, Singh M, Hruaikima L (2022) Control of structural damage on the rock mass characteristics and its influence on the rock slope stability along National Highway-07, Garhwal Himalaya, India: an ensemble of discrete fracture network (DFN) and distinct element method (DEM). Bull Eng Geol Env 81:96. https://doi.org/10.1007/s10064-022-02575-5

Stavropoulou M (2014) Discontinuity frequency and block volume distribution in rock masses. Int J Rock Mech Min Sci 65:62–74. https://doi.org/10.1016/j.ijrmms.2013.11.003

Taboni B, Umili G, Ferrero AM (2023) A design scenario approach for choosing protection works against rockfall phenomena. Remote Sens 15:4453. https://doi.org/10.3390/rs15184453

Toe D, Bourrier F, Forren LKA, Berger F (2018) A novel DEM approach to simulate block propagation on forested slopes. Rock Mech Rock Eng 51:811–825. https://doi.org/10.1007/s00603-017-1348-2

Torsello G, Vallero G, Castelli M (2021) The role of block shape and slenderness in the preliminary estimation of rockfall propagation. In: IOP Conference Series: Earth and Environmental Science, pp 833. https://doi.org/10.1088/1755-1315/833/1/012177

Umili G, Carriero MT, Taboni B, Migliazza MR, Ferrero AM (2024) A new analytical solution for calculating rock block volume. Rock Mech Rock Eng. https://doi.org/10.1007/s00603-023-03728-y

Umili G, Taboni B, Ferrero AM (2023) The influence on uncertainties: a focus on block volume and shape assessment aimed at rockfall analysis. J Rock Mech Geotech Eng 15(9):2250–2263. https://doi.org/10.1016/j.jrmge.2023.03.016

UNI—Ente Italiano di Normazione, 2019, UNI 11211-X Opere di difesa dalla caduta massi (*in italian*)

Volkwein A, Schellenberg K, Labiouse V, Agliardi F, Berger F, Bourrier F, Dorren L, Gerber W, Jaboyedoff M (2011) Rockfall characterization and structural protection—a review. Nat Hazards Earth Syst Sci 11(9):2617–2651. https://doi.org/10.5194/nhess-11-2617-2011

Wang H, Latham J-P, Poole A (1993) In-situ block size assessment from discontinuity spacing data. Int J Rock Mech Min SciGeomech Abstr 30(2):106. https://doi.org/10.1016/0148-9062(93)90982-J

Wang H, Latham J-PP, Poole AB (1991) Predictions of block size distribution for quarrying. Q J Eng Geol 24(1):91–99. https://doi.org/10.1144/GSL.QJEG.1991.024.01.10

Wang X, Cai M (2020) A DFN-DEM multi-scale modelling approach for simulating tunnel excavation response in jointed rock masses. Rock Mech Rock Eng 53:1053–1077. https://doi.org/10.1007/s00603-019-01957-8

Wyllie DC (2015) Rock fall engineering. CRC Press, New York

Yu Z, Luo L, Liu C, Guo L, Qi X, Zhao L (2021) Dynamic response of flexible rockfall barriers with different block shapes. Landslides 18(7):2621–2637. https://doi.org/10.1007/s10346-021-01658-w

Zhang L, Einstein HH (2000) Estimating the intensity of rock discontinuities. Int J Rock Mech Min Sci 37(5):819–837

Zhang Y, Liu X, Guo P, Jia P, Yang T, Ren F (2021) Numerical characterization of slope rock mass through considerations of hydraulic and mechanical properties. Landslides 18:2465–2481. https://doi.org/10.1007/s10346-021-01672-y

Zhou Z, Sun J, Lai Y, Wei C, Hou J, Bai J, Huang X, Liu H, Xiong K, Cheng S (2022) Study on size effect of jointed rock mass and influencing factors of the REV size based on the SRM method. Underg. Space Tech, Tunn. https://doi.org/10.1016/j.tust.2022.104613